Sand transport beneath waves: The role of progressive wave streaming and other free surface effects

Wouter M. Kranenburg,[1] Jan S. Ribberink,[1] Jolanthe J. L. M. Schretlen,[1] and Rob E. Uittenbogaard[2]

[1] Recent large-scale wave flume experiments on sheet-flow sediment transport beneath Stokes waves show more onshore-directed sediment transport than earlier sheet-flow experiments in oscillating flow tunnels. For fine sand, this extends to a reversal from offshore- (tunnels) to onshore (flumes)-directed transport. A remarkable hydrodynamic mechanism present in flumes (with free water surface), but not in tunnels (rigid lid), is the generation of progressive wave streaming, an onshore wave boundary layer current. This article investigates whether this streaming is the full explanation of the observed differences in transport. In this article, we present a numerical model of wave-induced sand transport that includes the effects of the free surface on the bottom boundary layer. With these effects and turbulence damping by sediment included, our model yields good reproductions of the vertical profile of the horizontal (mean) velocities, as well as transport rates of both fine and medium sized sediment. Similar to the measurements, the model reveals the reversal of transport direction by free surface effects for fine sand. A numerical investigation of the relative importance of the various free surface effects shows that progressive wave streaming indeed contributes substantially to increased onshore transport rates. However, especially for fine sands, horizontal gradients in sediment advection in the horizontally nonuniform flow field also are found to contribute significantly. We therefore conclude that not only streaming, but also inhomogeneous sediment advection should be considered in formulas of wave-induced sediment transport applied in morphodynamic modeling. We propose a variable time-scale parameter to account for these effects.

1. Introduction

[2] The development of cross-shore and long-shore coastal bottom profiles is strongly determined by the dynamics of water and sediment in the bottom boundary layer induced by surface waves. This has been the rationale for many experimental, analytical, and numerical studies on the interaction between wave motion and sand beds. Understanding of the interaction processes steers the development of parameterized sediment transport formulas that are feasible in large-scale morphodynamic simulations. Finally, these large-scale simulations provide insight into coastal bottom profile developments.

[3] A research topic of many wave-bed interaction studies is the influence of the wave shape on flow velocities, bed shear stresses, and sediment transport rates. These studies either focus on velocity skewness (present under waves with amplified crests), acceleration skewness (present under waves with steep fronts), or both phenomena in joint occurrence (for references, see *Ruessink et al.* [2009]). The experimental studies on wave-shape effects have been carried out in oscillating flow tunnels (with horizontally uniform flow), with both fixed and mobile flat beds of various sand grain sizes, and with special attention paid to the sheet-flow transport regime, where bed forms are washed away and the bed is turned into a moving sediment layer [*Ribberink et al.*, 2008]. An important observation from tunnel experiments in the sheet-flow regime is that under velocity-skewed flow over coarse grains, the sediment transport is mainly onshore, but net transport decreases with decreasing grain sizes and can even become negative [*O'Donoghue and Wright*, 2004]. An explanation for this is the phase-lag effect: rather fine sediment is stirred up by the strong onshore motion, settles only slowly, is still partly suspended during flow reversal, and is subsequently transported offshore

[1]Water Engineering and Management, University of Twente, Enschede, Netherlands.

[2]Deltares, Delft, Netherlands.

Corresponding author: W. M. Kranenburg, Water Engineering and Management, University of Twente, Box 7500 AE, Enschede, Netherlands. (w.m.kranenburg@utwente.nl)

[*Dohmen-Janssen et al.*, 2002]. Studies on the effect of acceleration skewness [e.g., *Van der A et al.*, 2011] have revealed that the increased acceleration during the onshore motion results in increased near-bed vertical velocity gradients and bed shear stresses. This enhances sediment pickup and net onshore transport. For purely acceleration-skewed oscillations over fine sand, the phase-lag effect also contributes to onshore transport: more time is available for settling subsequent to maximum onshore flow and less following maximum offshore flow.

[4] *Dohmen-Janssen and Hanes* [2002] and very recently *Schretlen* [2012] carried out detailed experiments on sand transport under velocity-skewed waves over flat beds in full-scale wave flumes. The flume experiments of *Dohmen-Janssen and Hanes* [2002] show larger transport rates for medium grain sizes compared to tunnel experiments with similar velocity skewness. *Schretlen* [2012] even found a reversed transport direction for fine sands in flumes (onshore) compared to tunnels (offshore). An explanation of the increased onshore transport brought up in these studies is "progressive wave streaming," an onshore-directed bottom boundary layer current under influence of vertical orbital motions in the horizontally nonuniform flow beneath progressive waves [*Longuet-Higgins*, 1953]: The vicinity of the bed affects the phase difference between the horizontal and vertical orbital velocities. This introduces a wave-averaged transport of horizontal momentum toward the bed that drives the onshore current. Note that this process acts opposite to the net current generated in a turbulent bottom boundary layer by a velocity-skewed or acceleration-skewed oscillation ("wave shape streaming"). The latter mechanism is due to wave shape–induced differences in time-dependent turbulence during the onshore and offshore phases of the wave, which causes a nonzero wave-averaged turbulent shear stress [*Trowbridge and Madsen*, 1984; *Ribberink and Al-Salem*, 1995; *Fuhrman et al.*, 2009]). We studied the streaming and the changing balance between the generation mechanisms for varying wave conditions above fixed beds in *Kranenburg et al.* [2012]. In this study, we investigate numerically to what extent progressive wave streaming can explain the differences in transport of both medium and fine sized sand between tunnel and flume experiments. Further questions are: What other processes are introduced by the progressive character of the free surface wave, and how do they influence sand transport for various grain sizes? A good understanding of the tunnel-flume differences is relevant, because many transport formulas used in morphodynamic computations in science and engineering are based on tunnel experiments and do not include the flume and prototype free surface effects. This study should therefore contribute to improvement of these formulas.

[5] Free surface effects have been included in earlier modeling studies. For example, *Gonzalez Rodriguez* [2009] predicted the contribution of progressive wave streaming to onshore transport by coupling a higher-order analytical boundary layer model with a bed-load transport formula. However, this concept cannot be applied to fine sand. *Henderson et al.* [2004] and *Hsu et al.* [2006] studied sandbar migration with a clear fluid (single-phase) fixed bed numerical boundary layer model with advection-diffusion formulation for suspended sediment concentrations. A similar model was used by *Holmedal and Myrhaug* [2009]

and *Blondeaux et al.* [2012], both of whom found significant differences in transport rates between tunnel- and sea-wave simulations. Although their results are qualitatively consistent with the experimental data, no specification of the progressive wave streaming contribution hereto or quantitative comparison with flume measurements was provided in these studies. Also, the single-phase studies mentioned earlier do not consider the details of the sediment pickup and the effects of high sediment concentrations on grain settling velocity and turbulence. However, sediment-induced turbulence damping can largely affect velocity profiles and transport rates, especially for fine sediment [see, e.g., *Winterwerp*, 2001 (for steady flow); *Conley et al.*, 2008; *Hassan and Ribberink* [2010] (oscillatory flow)]. *Yu et al.* [2010] studied progressive wave effects with a two-phase model that explicitly accounts for fluid-grain and grain-grain interactions within the sheet-flow layer. However, until now this model type has been validated only for large to medium grain sizes (>0.2 mm) [*Amoudry et al.*, 2008].

[6] Compared to the single-phase modeling studies above, this study has three innovative aspects. First, we use a model that includes both free surface effects and sediment-related reduction of turbulence and settling velocities. Second, we present an extensive quantitative model validation on boundary layer flow beneath full-scale waves over a mobile bed, as well as on net transport of both fine and medium sediment in both tunnel and flume experiments. This detailed validation could be carried out only because detailed full-scale flume measurements became available recently [*Schretlen*, 2012]. A third new aspect is the differentiation between transport related to progressive wave streaming and related to other free surface effects, which we use to develop parameterizations for practical transport formulas.

[7] The outline of this article is as follows: section 2 describes our numerical model. The data used for model validation and the validation itself are described in section 3. Section 4 describes the model experiments quantifying the contribution of various free surface effects. The results are discussed in section 5, with a focus on their relevance for sediment transport formulas used in morphodynamic modeling. Our major conclusions are summarized in section 6.

2. Model Formulation

[8] Our model can be classified as a 1DV Reynolds averaged Navier-Stokes flat-bed boundary layer model with k-ε closure for turbulence and an advection-diffusion formulation for suspended sediment. It is an extension of the hydrodynamic model described by *Kranenburg et al.* [2012] with a sediment balance and feedback of sediment on the flow. The sediment formulations correspond to those in the previous model version used by *Ruessink et al.* [2009], originally developed by *Uittenbogaard et al.* [2001], now extended with advective terms. The main differences with *Henderson et al.* [2004], *Holmedal and Myrhaug* [2009], and *Blondeaux et al.* [2012] appear in the turbulence formulations (stratification effects) and, in the latter two cases, in the forcing of the model.

2.1. Basic Equations

[9] The fundamental unknowns solved by the model are horizontal flow velocity u, vertical flow velocity w, sediment concentration c, and turbulent kinetic energy k, and its rate

of dissipation ε. The flow velocities are solved from the following equations:

$$\frac{\partial u}{\partial t} + u\frac{\partial u}{\partial x} + w\frac{\partial u}{\partial z} = -\frac{1}{\rho_w}\frac{\partial p}{\partial x} + \frac{\partial}{\partial z}\left\{(\upsilon + \upsilon_t)\frac{\partial u}{\partial z}\right\} \tag{1}$$

$$\frac{\partial u}{\partial x} + \frac{\partial w}{\partial z} = 0 \tag{2}$$

where p is the pressure, ρ_w is the fluid density, υ is the kinematic viscosity of water, υ_t is the turbulence viscosity, and x and z are the horizontal and vertical coordinates, positive in onshore and upward direction, respectively.

[10] The closure for υ_t is provided by a k-ε model [*Rodi*, 1984], where k is the turbulent kinetic energy, ε is the energy dissipation rate, and their relation to υ_t:

$$\upsilon_t = c_\mu \frac{k^2}{\varepsilon} \tag{3}$$

[11] The turbulence quantities are solved from the following equations:

$$\frac{\partial k}{\partial t} + u\frac{\partial k}{\partial x} + w\frac{\partial k}{\partial z} = \frac{\partial}{\partial z}\left\{\left(\upsilon + \frac{\upsilon_t}{\sigma_k}\right)\frac{\partial k}{\partial z}\right\} + P_k - \varepsilon - B_k \tag{4}$$

$$\frac{\partial \varepsilon}{\partial t} + u\frac{\partial \varepsilon}{\partial x} + w\frac{\partial \varepsilon}{\partial z} = \frac{\partial}{\partial z}\left\{\left(\upsilon + \frac{\upsilon_t}{\sigma_\varepsilon}\right)\frac{\partial \varepsilon}{\partial z}\right\} + \frac{\varepsilon}{k}(c_{1\varepsilon}P_k - c_{2\varepsilon}\varepsilon - c_{3\varepsilon}B_k) \tag{5}$$

where P_k is the turbulence production, and B_k is the buoyancy flux. σ_k, σ_ε, c_μ, $c_{1\varepsilon}$, and $c_{2\varepsilon}$ are constants. We apply $(\sigma_k, \sigma_\varepsilon, c_\mu, c_{1\varepsilon}, c_{2\varepsilon}) = (1.0, 1.3, 0.09, 1.44, 1.92)$ (standard values, *Rodi* [1984]). The production term P_k yields

$$P_k = \upsilon_t\left(\frac{\partial u}{\partial z}\right)^2 \tag{6}$$

[12] The buoyancy flux B_k accounts for the conversion of turbulent kinetic energy to mean potential energy (or vice versa) with the mixing of sediment, treated equivalent to buoyancy flux in a salt-stratified or thermally stratified flow. In a stable stratification ($\partial \rho/\partial z < 0$), this flux will lead to turbulence reduction, in case of an unstable stratification to turbulence generation. Besides, in the latter case, the upward jets (by Rayleigh-Taylor instabilities) from the lighter fluid into the denser fluid on top of it produce extra vorticity, which is, considering the parallel between vorticity and ε (energy dissipation), accounted for by an increase of ε. This is described with the following expressions for the buoyancy flux B_k, the Brunt-Väisälä frequency N, and $c_{3\varepsilon}$:

$$B_k = \frac{\upsilon_t}{\sigma_p}N^2; \quad N^2 = -\frac{g}{\rho_m}\frac{\partial \rho_m}{\partial z}; \quad c_{3\varepsilon} = \begin{cases} 0 & N^2 \geq 0 \\ 1 & N^2 < 0 \end{cases} \tag{7}$$

where σ_p is a constant, in this case, equal to the turbulence Prandtl-Schmidt number σ_t for conversion of turbulence viscosity υ_t into eddy diffusivity of sediment; g is the gravitational acceleration; and ρ_m is the density of the local water-sediment mixture $\rho_m = \rho_w + (\rho_s - \rho_w)c$.

[13] The sediment (volume) concentration c is solved from a sediment balance:

$$\frac{\partial c}{\partial t} + u\frac{\partial c}{\partial x} + w\frac{\partial c}{\partial z} = \frac{\partial w_s c}{\partial z} + \frac{\partial}{\partial z}\left\{\left(\upsilon + \frac{\upsilon_t}{\sigma_t}\right)\frac{\partial c}{\partial z}\right\} \tag{8}$$

where we apply $\sigma_t = 0.7$ (as derived from experiments by *Breugem* [2012]). The local sediment fall velocity w_s is determined using the undisturbed settling velocity $w_{s,0}$ according to *Van Rijn* [1993], with a correction for hindered settling in high sediment concentrations following *Richardson and Zaki* [1954]:

$$w_s = w_{s,0}\left(1 - \frac{c}{c_s}\right)^p; \tag{9a}$$

$$w_{s,0} = \frac{10\upsilon}{d_{50}}\left[\left(1 + \frac{0.01\Delta g d_{50}^3}{\upsilon^2}\right)^{1/2} - 1\right] \text{ for } 0.1\text{mm} < d_{50} < 1.0\text{mm} \tag{9b}$$

with $c_s = 0.65$, $p = 5$, and $\Delta = (\rho_s - \rho_w)/\rho_w$.

[14] Assuming uniformity of wave shape and height during propagating over the horizontal sand bed, the model is reduced to a 1DV model by transformation of horizontal gradients of velocity, turbulence properties, and sediment concentration into time derivatives, using

$$\frac{\partial \ldots}{\partial x} = -\frac{1}{c_p}\frac{\partial \ldots}{\partial t} \tag{10}$$

where c_p is the wave propagation speed.

[15] The consideration of advective transport of horizontal momentum, turbulence properties, and sediment marks the fundamental difference between modeling the horizontally uniform situation like in oscillating flow tunnels or the horizontally nonuniform situation beneath progressive surface waves in prototype situation and wave flumes. The progressive wave streaming is driven by the wave-averaged vertical advective transport of horizontal momentum into the wave boundary layer (wave Reynolds stress).

2.2. Forcing

[16] The model can be forced in two ways. In the "match model" formulation, the principally unknown $u(t,z)$ is forced to match a predefined horizontal velocity signal at a certain vertical level, e.g., a measured time series. The associated (oscillating plus mean) pressure gradient is determined iteratively every time step from equation (1) at the matching level. In the alternative "free model" formulation, the oscillating horizontal pressure gradient is determined in advance from a given free stream horizontal velocity $\tilde{u}_\infty$ (or u_{red}) with zero mean, using:

$$-\frac{1}{\rho}\frac{\partial \tilde{p}}{\partial x} = \frac{\partial \tilde{u}_\infty}{\partial t} + \tilde{u}_\infty\frac{\partial \tilde{u}_\infty}{\partial x} \tag{11}$$

[17] In the latter approach, mass transport arising from streaming mechanisms and Stokes's drift is not compensated by a return flow driven by an additional mean pressure gradient, and the mean current is allowed to develop freely. This formulation needs a predefined oscillating free stream velocity as input.

2.3. Boundary Conditions

[18] To solve equations (1), (4), and (5), we apply the upper boundary conditions:

$$\upsilon_t \frac{\partial u}{\partial z}\bigg|_{z=top} = 0; \qquad \frac{\partial k}{\partial z}\bigg|_{z=top} = 0; \qquad \frac{\partial \varepsilon}{\partial z}\bigg|_{z=top} = 0 \qquad (12)$$

and the lower boundary conditions:

$$\frac{\partial u}{\partial z}\bigg|_{z=0} = \frac{u_*}{9kz_0}; \qquad k\bigg|_{z=0} = \frac{u_*^2}{\sqrt{c_\mu}}; \qquad \varepsilon\bigg|_{z=0} = \frac{u_*^3}{9kz_0} \qquad (13)$$

[19] Here, u_* is the friction velocity, $\kappa = 0.41$ is the von Karman constant, and z_0 is the roughness height. The lower boundary conditions assume hydraulically rough turbulent flow near the bed and are applied at a fixed bottom level. We relate z_0 to the median sand grain size d_{50} by applying Nikuradse roughness height $k_N = 2d_{50}$ and $z_0 = k_N/30$.

[20] The sediment balance of equation (8) is solved using a no-flux condition at the top boundary and a pickup function at reference height $z = z_a = 2d_{50}$. The latter reads:

$$w_s c_b + \left(\upsilon + \frac{\upsilon_t}{\sigma_t}\right)\frac{\partial c}{\partial z}\bigg|_{z=z} = 0 \qquad (14)$$

[21] For the reference concentration c_b, we use the expression of *Zyserman and Fredsoe* [1994]:

$$c_b(t) = \frac{0.331(\theta - \theta_c)^{1.75}}{1 + \frac{0331}{C_m}(\theta - \theta_c)^{1.75}} \qquad (15)$$

a function of the instantaneous Shields parameter θ, the critical Shields parameter θ_c for initiation of motion [*Van Rijn*, 1993], and a constant C_m, set to 0.32 for oscillatory flow [*Zyserman and Fredsoe*, 1994]. This reference concentration expression is an empirical relation originally based on near-bed concentration measurements in steady flow and the assumption of Rouse concentration profiles for suspended sediment. In the thin layer beneath $z = z_a$, we apply $c(z) = c|_{z=z_a}$.

3. Validation

[22] The validation of the model consists of four parts. We first investigate the quality of the model in reproducing boundary layer flow above a mobile bed (section 3.2). Because of our interest in the role of streaming in explaining the different trends in observed sediment transport rates in flumes and tunnels, we focus hereby especially on the mean current. Subsequently, we compare model and data for net sediment transport rates (section 3.3). A separate section is dedicated to the model reproduction of the observed different trends in transport as function of velocity moments (section 3.4). Finally, we conclude the validation with a sensitivity analysis and discussion (section 3.5). This section starts with a description of the experimental data used in the model validation (section 3.1).

3.1. Experimental Data for Model Validation

[23] The model-data comparison on flow velocities is carried out with data from the full-scale wave flume experiments

described by *Schretlen et al.* [2011] and *Schretlen* [2012]. In these recent experiments, regular trochoidal waves of varying wave period T and wave height H were sent through a 280 m long wave flume with water of 3.5 m depth above a horizontal sand bed with a median grain size d_{50} of 0.245 and 0.138 mm, respectively. At the end, the waves were absorbed by a dissipative beach. Multiple experimental runs (both 30 and 60 minute runs) were carried out for each wave condition. At 110 m from the wave generator, a frame with various instruments was fixed to the flume wall, among them an ultrasonic velocity profiler (UVP) that was used to obtain detailed vertical profile measurements of the velocity inside the wave boundary layer. This makes these experiments the first that offer detailed information on the boundary layer flow beneath full-scale waves over a mobile, flat bed. Before and after each run, the horizontal profile of the bed was measured either with a rolling bed profiler or with echo sounders (four next to each other to average out transversal variations). Subsequently, net sediment transport rates $<q_s>$ (m^2/s) at the position of the instrument frame (x_2) were determined from sand volume conservation by spatial integration of the changes in bed level z_b between successive profile measurements:

$$\langle q_s \rangle_{x2} = -\int_{x1}^{x2} \frac{\partial((1-\varepsilon)z_b)}{\partial t} dx \qquad (16)$$

[24] This integration started at x_1, a location with zero transport in a fixed bed zone offshore. Because the value and potential variation of porosity ε during the tests were unknown, a constant value of $\varepsilon = 0.4$ was assumed following *Dohmen-Janssen and Hanes* [2002]. Repetition of the procedure for the multiple experimental runs resulted in an average transport rate and standard deviation for each condition.

[25] In addition to transport rates from *Schretlen* [2012], the model-data comparison on sediment transport also includes transport rates from the full-scale wave flume experiments of *Dohmen-Janssen and Hanes* [2002]. In these experiments, again, T and H of the nearly conoidal waves were varied, and water depth h was 3.5 m. The horizontal sand bed consisted of well-sorted grains with $d_{50} = 0.240$ mm, and the horizontal velocities were measured with an acoustic Doppler velocimeter at around 100 mm above the still bed level. To the best of our knowledge, we thus include all available transport rates from full-scale wave flume experiments on sheet-flow sand transport beneath regular waves. Considering the discussion on different trends in transport between flume and tunnel experiments, tunnel experiments on transport of fine ($d_{50} \leq 0.140$ mm) and medium sized ($d_{50} \geq 0.210$ mm) sand beneath velocity skewed oscillatory flow also have been included in the model validation. An overview of all the data used is given in Table 1. This table gives the names of the various conditions as used by the original authors, the period T, median grain size d_{50}, measured transport rates $<q_s>$, and a characterization of the flow velocities at $z = z_{match}$, where z_{match} is the level at which the model will be forced to match the measured velocities. Note that flow and transport information generally concern averaged values over multiple runs per condition. For the experiments of *Schretlen* [2012], standard deviations are given in Table 2.

Table 1. Overview of Simulated Experiments[a,b,c]

Experiment[d,e,f,g]	Condition	T (s)	d_{50} (mm)	z_{match} (mm)	U_0 (m/s)	$u_{on,red}$ (m/s)	$u_{off,red}$ (m/s)	R_{red} (-)	u_{rms} (m/s)	$\langle u^3 \rangle$ (m³/s³)	$\langle u_{red}^3 \rangle$ (m³/s³)	θ_{max} (-)	w_s/u^* (-)	$q_{s,meas}$ (10⁻⁶ m²/s)	$q_{s,comp\ (closed)}$ (10⁻⁶ m²/s)	$q_{s,comp\ (open)}$ (10⁻⁶ m²/s)
1	1265m	6.5	0.245	40	−0.042	1.41	−0.84	0.63	0.78	0.216	0.287	2.04	0.49	29.7	63.1	81.3
2	1550m	5.0	0.245	40	0.002	1.28	−0.97	0.57	0.79	0.145	0.138	1.76	0.47	32.9	44.0	66.6
3	1565m	6.5	0.245	40	−0.017	1.60	−0.91	0.64	0.88	0.402	0.430	2.55	0.44	64.8	96.3	117.5
4	1575m	7.5	0.245	40	−0.084	1.53	−0.70	0.69	0.72	0.239	0.362	2.36	0.53	42.3	65.0	71.5
5	1065f	6.5	0.138	40	−0.024	1.14	−0.78	0.59	0.66	0.091	0.123	2.16	0.25	19.7	40.4	47.0
6	1265f	6.5	0.138	40	−0.042	1.23	−0.73	0.63	0.68	0.119	0.178	2.49	0.24	37.5	35.5	42.3
7	1550f	5.0	0.138	40	−0.027	1.31	−1.05	0.56	0.83	0.077	0.135	2.87	0.20	40.7	81.0	96.8
8	1565f	6.5	0.138	40	−0.073	1.56	−0.84	0.65	0.82	0.239	0.387	3.84	0.20	51.6	44.9	53.8
9	1575f	7.5	0.138	40	−0.106	1.61	−0.70	0.70	0.77	0.232	0.417	4.04	0.22	69.5	53.4	63.5
10	MI	6.5	0.240	103	−0.045	1.02	−0.74	0.58	0.59	0.035	0.081	1.16	0.61	33.8	21.3	22.7
11	MH	6.5	0.240	109	−0.046	1.14	−0.62	0.65	0.62	0.095	0.147	1.43	0.59	42.9	36.9	34.8
12	MF	9.1	0.240	99	−0.030	1.30	−0.64	0.67	0.65	0.172	0.209	1.69	0.58	76.7	60.8	53.9
13	ME	9.1	0.240	99	−0.052	1.49	−0.58	0.72	0.68	0.246	0.317	2.20	0.56	107.3	84.7	75.6
14	B7	6.5	0.210	200	0.048	0.90	−0.55	0.62	0.50	0.105	0.069	1.03	0.60	12.4	17.7	9.6
15	B8	6.5	0.210	200	0.038	1.27	−0.74	0.63	0.70	0.257	0.202	1.90	0.44	38.9	46.5	31.6
16	B10	9.1	0.210	200	0.020	0.94	−0.55	0.63	0.55	0.099	0.081	1.02	0.57	18.6	20.5	12.0
17	B11	9.1	0.210	200	0.022	1.23	−0.71	0.63	0.71	0.215	0.182	1.64	0.45	44.8	53.6	36.2
18	B13	6.5	0.210	200	0.010	1.19	−0.91	0.57	0.70	0.130	0.115	1.67	0.44	21.0	22.8	17.9
19	B14	9.1	0.210	200	−0.064	1.25	−0.86	0.59	0.76	0.055	0.166	1.69	0.42	22.0	35.2	33.4
20	B15	5.0	0.210	200	0.030	0.95	−0.57	0.63	0.51	0.105	0.082	1.22	0.57	15.2	17.9	11.5
21	B16	12.0	0.210	200	0.005	1.03	−0.64	0.62	0.56	0.105	0.100	1.14	0.58	20.0	25.7	15.7
22	C9	6.5	0.210	98	0.000	1.05	−0.66	0.62	0.56	0.108	0.108	1.37	0.54	20.5	21.4	17.0
23	C11	6.5	0.210	108	−0.023	1.40	−0.84	0.63	0.80	0.218	0.262	2.23	0.39	51.5	37.7	30.6
24	MA5010	5.0	0.270	80	0.030	1.38	−0.91	0.60	0.83	0.293	0.231	1.89	0.50	53.0	44.2	29.0
25	MA7515	7.5	0.270	80	0.000	1.44	−0.94	0.61	0.86	0.266	0.266	1.86	0.51	36.0	59.7	43.1
26	D11	6.5	0.128	250	0.019	0.98	−0.61	0.62	0.56	0.106	0.088	1.75	0.25	9.0	6.7	6.6
27	D12	6.5	0.128	250	0.062	1.54	−1.00	0.61	0.91	0.478	0.324	3.90	0.16	−228.3	−107.5	−113.9
28	D13	6.5	0.128	250	0.041	1.26	−0.80	0.61	0.73	0.247	0.182	2.73	0.20	−30.2	−42.0	−37.9
29	D14	6.5	0.128	250	0.017	0.77	−0.50	0.61	0.45	0.052	0.042	1.14	0.31	7.6	10.2	8.1
30	LA406	4.0	0.130	35	−0.005	1.17	−0.73	0.62	0.70	0.151	0.159	2.59	0.20	−8.1	−12.7	−27.3
31	LA612	6.0	0.130	35	−0.029	1.37	−0.88	0.61	0.85	0.227	0.289	3.13	0.18	−61.0	−49.1	−83.6
32	FA5010	5.0	0.130	80	0.030	1.38	−0.91	0.60	0.83	0.293	0.231	3.33	0.18	−128.0	−57.0	−71.4
33	FA7515	7.5	0.130	80	0.000	1.44	−0.94	0.61	0.86	0.266	0.266	3.32	0.18	−88.0	−72.5	−88.9

[a]Definitions for the used velocity parameters: U_0, wave-averaged horizontal velocity; u_{red}, reduced velocity; u_{red} reduced velocity signal, i.e., the oscillating part of the velocity only $(u(t) - U_0)$; $u_{on,red}$ and $u_{off,red}$, maximum onshore respectively offshore value of u_{red}; R_{red}, velocity skewness measure computed from u_{red} with $R_{red} = u_{on,red}/(u_{on,red} + u_{off,red})$; u_{rms}, root mean square of the complete velocity signal; $\langle u^3 \rangle$, third-order velocity moment of the complete velocity signal; $\langle u_{red}^3 \rangle$, third-order velocity moment of the reduced velocity signal.

[b]Shields parameter $\theta_{max} = 1/2 f_w u_{on,red}^2 (\Delta g d_{50})^{-1}$, with f_w following *Swart* [1974], and $k_N = 2 d_{50}$.

[c]Other dimensionless parameter $w_s/u^* = w_s(f_w)^{-1/2} u_{rms}^{-1}$ with w_s from equation (9b); suspension parameter $w_s/u^* = w_s(f_w)^{-1/2} u_{rms}^{-1}$ with w_s from equation (9b), f_w following *Swart* [1974], and $k_N = 2 d_{50}$.

[c]Other dimensionless parameter ranges: 1e3 < A/k_N < 6e3; 4e5 < RE < 2e6 and 1.5e2 < Ψ < 8e2 with $A = \sqrt{2} u_{rms} \omega^{-1}$, $RE = A \sqrt{2} u_{rms} \nu^{-1}$, and mobility number $\Psi = 2 u_{rms}^2 (\Delta g d_{50})^{-1}$.

[d]Experiments 1 to 13 are flume experiments; experiments 14 to 33 are tunnel experiments.

[e]Original publication: experiments 1–9: *Schretlen* [2012]; 10–13: *Dohmen-Janssen and Hanes* [2002]; 14–21: *Ribberink and Al-Salem*, [1994]; 22 and 23: *Ribberink and Al-Salem* [1995]; 24, 25, 32, 33: *O'Donoghue and Wright* [2004]; 26–29: *Ribberink and Chen* [1993]; 30, 31: *Wright* [2002].

[f]Explanation of nomenclature 1–9: XXYYm/f means waves with (at the wave generator) H = XX/10 m and T = YY/10 s over a bed of medium or fine sized sand.

[g]All flume experiments (1–13) were carried out in water with a depth of 3.5 m.

Table 2. Standard Deviations of Velocity and Transport Parameters for the *Schretlen* [2012] Experiments and Accompanying Simulations

Experiment	Condition	n^{a}	U_0 (m/s)	$U_{on,red}$ (m/s)	$U_{off,red}$ (m/s)	R_{red} (-)	u_{rms} (m/s)	$<u^3>$ (m³/s³)	$<u^3_{red}>$ (m³/s³)	$q_{s,meas}$ (other n) (10^{-6} m²/s)	$q_{s,comp}$ (closed) (10^{-6} m²/s)	$q_{s,comp}$ (open) (10^{-6} m²/s)
1	1265m	5	0.044	0.17	0.09	0.01	0.09	0.124	0.098	13.4	28.0	32.2
2	1550m	7	0.034	0.13	0.15	0.02	0.10	0.079	0.029	20.4	15.1	26.9
3	1565m	4	0.034	0.18	0.08	0.01	0.09	0.220	0.146	11.2	38.2	37.4
4	1575m	4	0.027	0.10	0.07	0.01	0.04	0.084	0.063	13.0	16.8	15.5
5	1065f	3	0.008	0.04	0.03	0.00	0.02	0.006	0.010	1.8	2.0	4.0
6	1265f	7	0.011	0.11	0.09	0.01	0.06	0.047	0.049	2.8	6.3	6.7
7	1550f	4	0.011	0.04	0.05	0.01	0.03	0.020	0.014	4.3	12.4	18.4
8	1565f	5	0.024	0.13	0.12	0.02	0.08	0.077	0.097	10.2	8.8	11.1
9	1575f	2	0.003	0.06	0.07	0.01	0.04	0.010	0.034	7.1	4.6	0.3

[a]Number of UVP-velocity signals, also input to n simulations.

3.2. Model-Data Comparison on Horizontal Velocities

[26] For model-data comparison on boundary layer flow, we simulate the experiments of *Schretlen* [2012] by forcing the model at $z = z_{match}$ with the UVP-measured velocity at that level, and compare model and data for the flow underneath. Except for the few runs for which the UVP data did not extend up to there, we choose the matching level z_{match} at 40 mm above the initial still bed level ($z = 0$ mm). Figure 1 presents measured and simulated horizontal velocities for a single run of condition 1065f (harmonic representation).

[27] The results for amplitude and phase of the harmonic components, especially components 1 and 2, show that the model gives a good reproduction of the wave boundary layer thickness: The levels of maximum amplitude in data and model results nearly coincide, and model and data show a similar level for the start of the phase lead of the boundary layer flow. A typical characteristic of sheet flow beneath velocity-skewed waves is deeper mobilization of the bed during the onshore movement compared to the offshore movement (erosion-depth asymmetry). This results in distinct onshore wave-averaged velocities U_0 in the lower part of the sheet-flow layer, which increase with increasing velocity skewness. This onshore mean velocity below the initial bed level is also visible in the shown data. The present model has a fixed bottom level and will therefore not reproduce this specific feature. However, the reproduction of magnitude, direction, and shape of the U_0 profile higher up in the wave boundary layer is remarkably good. To illustrate the quality of this reproduction and the added value of the present model formulations compared to models in the literature, we compare the present model (BL2-SED) with results from, respectively, the first-order "tunnel" version (BL1-SED) and the purely hydrodynamic version of the present model (BL2-HYDRO) discussed in *Kranenburg et al.* [2012]. The results of the latter are expected to be comparable
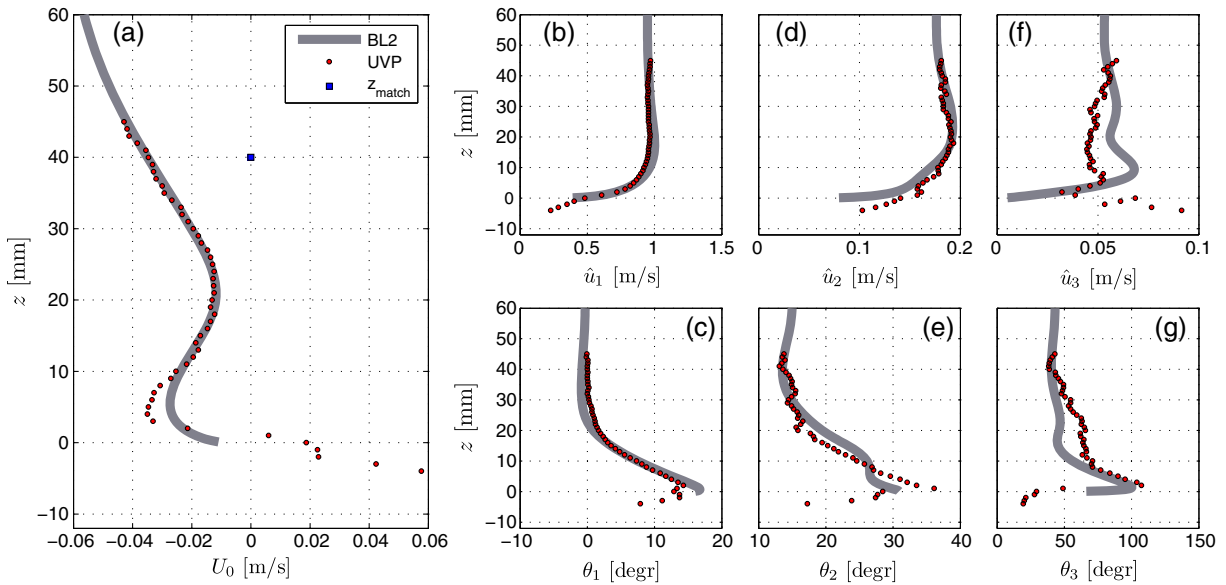

Figure 1. (a) Wave-averaged velocity U_0 and (b, d, f) amplitudes $\hat{u}$ and (c, e, g) phases θ of first, second, and third harmonic components of the horizontal velocity. Dots represent experimental data from *Schretlen* [2012] (condition 1065f: regular velocity-skewed waves with $H = 1.0$ m, $T = 6.5$ s, $h = 3.5$ m, and $d_{50} = 0.138$ mm). Gray lines represent model results; squares represent matching level. Positive velocities are directed onshore.

with *Henderson et al.* [2004], a second-order boundary layer model without feedback of sediment on the flow. For the three model versions, the mismatch between model and data, averaged over the domain between $z = z_{match}$ and $z = 0$ mm, computed discretely by

$$\frac{1}{z_{match}} \int_{z=0}^{z=z_{match}} \sqrt{\left(U_{0,comp}(z) - U_{0,meas}(z)\right)^2} dz \qquad (17)$$

is, respectively, 0.0292 m/s (BL1-SED), 0.0079 m/s (BL2-HYDRO), and 0.0024 m/s (BL2-SED). The present model not only has by far the smallest averaged mismatch, Figure 2 shows that it also gives a better reproduction of the shape of the current profile. We therefore conclude that both progressive wave streaming and feedback of sediment on the flow through stratification effects need to be considered to model
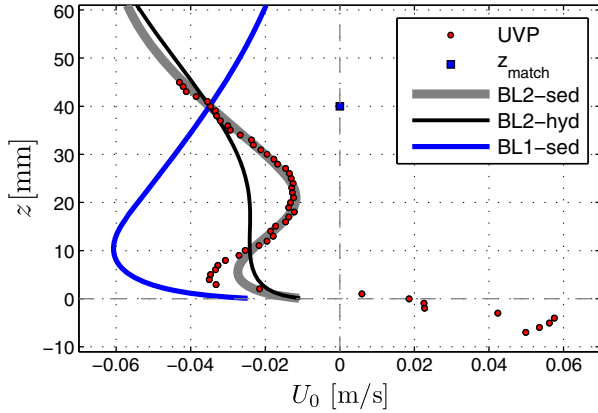
Figure 2. Wave-averaged horizontal velocity U_0. Red dots represent experimental data. Lines represent simulation with BL1-SED, the first-order boundary layer model with suspended sediment, with BL2-HYDRO, the second-order boundary layer model without feedback of sediment on the flow, and with BL2-SED, the present second-order boundary layer model with suspended sediment. Conditions are as in Figure 1.

the net current in the boundary layer under waves above a mobile bed and to study the influence of streaming on sediment transport.

[28] Figure 3 shows U_0 profiles for experimental conditions with varying H, T, and d_{50}. The changes in U_0 for changing H, T, and d_{50} in the six runs shown here are representative for the H, T, and d_{50} dependency in all other runs, as can be verified for U_0 at z_{match} from Table 1. These results show that also for different wave and bed conditions the model is rather well able to reproduce the magnitude and shape of the U_0 profile, and also shows an H, T, and d_{50} dependency comparable to the data. (Compare, e.g., the changes in local minima and maxima with changing H and T). For more discussion on the shape of the U_0 profiles, the influence thereon of wave-shape streaming, progressive wave streaming, and Stokes drift compensation, and the changing balance between these mechanisms for changing wave and bed conditions, we refer to *Kranenburg et al.* [2012] and *Schretlen* [2012].

3.3. Model-Data Comparison on Sediment Transport

[29] Next, we compare computed and measured net sediment transport rates. Note that not every experimental run of *Schretlen* [2012] resulted in successful measurement of both velocity and sediment transport. To include as much experimental information as possible, the setup of the comparison is as follows: for each run with successful UVP measurements, a simulation is carried out, using the UVP-measured velocity signal at $z = z_{match}$ to drive the model. All these simulations result in a single computed net sediment transport rate. Per wave condition, we determine mean and standard deviation of the computed transport rates and compare these with the mean and standard deviation of the experimentally determined transport rates. Note that the latter thus also includes runs for which no UVP measurements are available, whereas the computed results also include runs for which no transport rate could be determined from the experiments. The flume experiments of *Dohmen-Janssen and Hanes* [2002] ($d_{50} = 0.240$ mm) are simulated by driving the model with the acoustic Doppler velocimeter–measured horizontal velocities at around 100
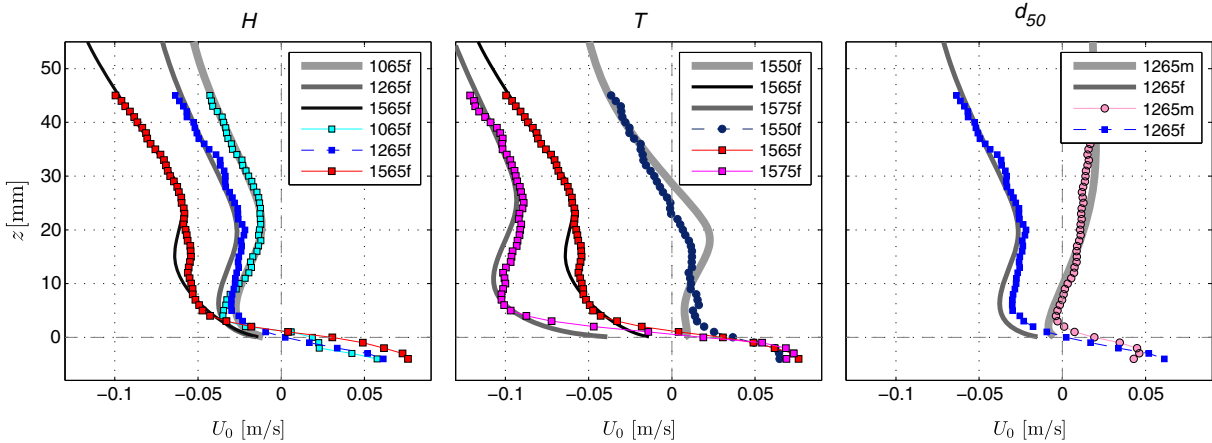
Figure 3. Measured and computed profiles of period-averaged horizontal velocity U_0 for various wave and bed conditions: (a) for waves with height H of 1.0, 1.2, and 1.5 m; (b) for waves with period T of 5.0, 6.5, and 7.5 s; (c) for waves over beds with a median grain size d_{50} of 0.138 (f, fine) and 0.245 mm (m, medium).

mm above the still bed level (i.e., around 2.5 times the UVP-matching level). For these experiments, no velocity data are available closer to the bed, and per condition only one time series of horizontal velocities is available. As a consequence, the computed net transport for these conditions is based on one simulation only, whereas the measured transport is an average over multiple experimental runs. The model-data comparison on net transport rates $<q_s>$ is shown in Figure 4a. Figure 4b extends Figure 4a with simulations of tunnel experiments on transport of both fine ($d_{50} \leq 0.140$ mm) and medium ($d_{50} \geq 0.210$ mm) sand under velocity-skewed oscillations. The (mean) computed net transport rates per condition have been added to Table 1. For the conditions of *Schretlen* [2012], standard deviations have been added to Table 2.

[30] We observe from Figure 4 that the direction of $<q_s>$ is reproduced correctly in all cases. For nearly all cases, the model prediction is within a factor 2 of the measured $<q_s>$. It is shown in Figure 4a that within the various sets of wave flume experiments, trends of increasing transport are also reproduced, except for condition 1065f, 1550f, and 1265m. For each set, a score has been given to the reproduction by averaging S over all cases within the set, with

$$S = 1 - \frac{|q_{s,c} - q_{s,m}|}{|q_{s,c} + q_{s,m}|} \tag{18}$$

[31] This measure results in identical scores for overprediction with a factor of 2 and underprediction with a factor of 1/2 (namely, 0.667), and results in negative values when the transport direction is not reproduced well. The results per set are added to Figure 4, and all lie between 0.77 and 0.88 (around factor of 1.6 and 1.3), which is considered a good quantitative reproduction for sediment transport rates [*Davies et al.*, 2002]. The model overpredicts the medium sand flume experiments of *Schretlen* [2012] (circles in Figure 4, $<S> = 0.77$), whereas it slightly underpredicts the medium sand flume experiments of *Dohmen-Janssen and Hanes* [2002] (diamonds in Figure 4, $<S> = 0.87$). An explanation for this systematic difference might be the wider sieve curve of the sand in the experiments of *Schretlen* [2012], a difference not present in the simulations because the model considers the median grain size only. Finally, note that for the medium sand flume experiments of *Schretlen* [2012], the differences between the various runs of a condition are rather large. This experimental scatter is present both for the UVP-measured velocities (input to the model) and the measured (and computed) transport rates (see Table 2).

3.4. Transport Against Velocity Moments

[32] An important observation from tunnel experiments with velocity-skewed oscillatory flows is that the net transport rate of medium sized sand ($d_{50} \geq 0.2$ mm) is proportional to the third-order moment of the horizontal velocity in the free stream: $<q_s> \sim <u^3>$ [*Ribberink and Al-Salem*, 1994]. This relation, an indication for quasi-steady behavior of $<q_s>$ during the wave cycle [see, e.g., *Bailard*, 1981] is not valid for finer sands [*O'Donoghue and Wright*, 2004]. In that case, phase-lag effects will play a role, and instantaneous concentration and intrawave transport are no longer coupled to the instantaneous free stream velocity. Net transport rates can even become negative for increasing positive velocity moments $<u^3>$. In wave flume experiments, the $<q_s> \sim <u^3>$ relation for medium sized sand is also found [*Dohmen-Janssen and Hanes*, 2002]. However, *Schretlen* [2012] shows that the reversal of transport direction for fine
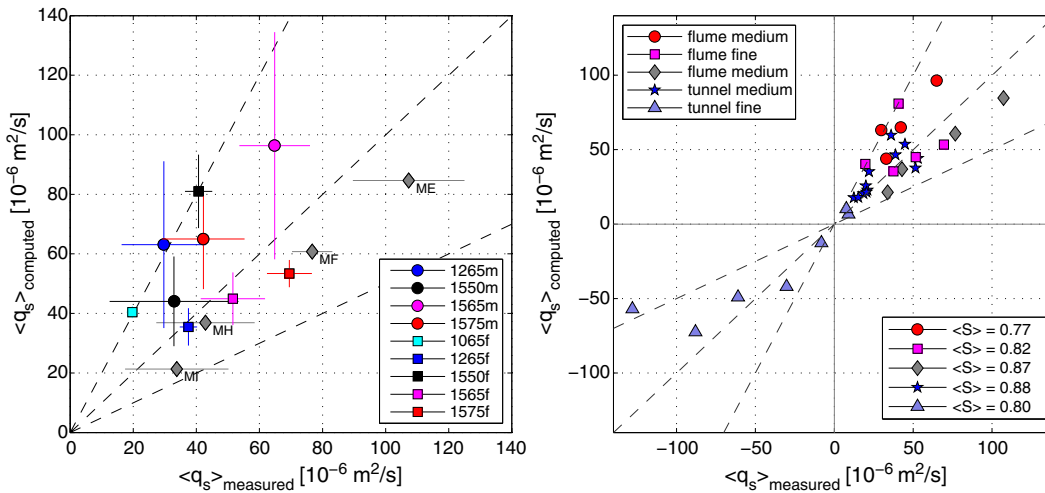
Figure 4. Computed against measured net sediment transport rates $<q_s>$ under regular, predominantly velocity-skewed waves. (left) For all available full-scale flume experiments, with standard deviations; (right) for both flume and tunnel experiments. Circles represent *Schretlen*'s [2012] flume experiments with medium sized sand (1–4 in Table 1); squares represent *Schretlen*'s [2012] flume experiments with fine sand (5–9); diamonds represent *Dohmen-Janssen and Hanes*'s [2002] flume experiments with medium sized sand (10–13); stars represent tunnel experiments with medium sand (14–25); triangles represent tunnel experiments with fine sand (26–33). A total of 33 conditions and 65 simulations (note that condition 27 falls outside the graph). Dashed lines: $y = \alpha x$, for α is 1/2, 1, and 2; $<S>$ gives a reproduction quality measure per set, see equation (18).

sand is absent. Before we apply the model to investigate physical explanations of these differences, we need to verify the model reproduction of these trends.

[33] In Figure 5, $<q_s> \sim <u^3>$ trends from experiments (column 1) are compared with the simulation results (column 2), both for medium (row a) and fine (row b) sand, and for tunnel and flume conditions (different symbols). We choose to determine the third-order velocity moment from the oscillating part of the horizontal velocities only ($u_{red} = u(t) - U_0$, see Table 1). The reason is that $<u^3>$ is sensitive for U_0 variations, whereas U_0 depends on the height of the velocity measurements (much more than the oscillating velocity, see, e.g., Figure 1) and is itself affected by the differences between flume and tunnel. In this way, differences in z_{match} between the various experiments will not influence the trends, and tunnel and flume experiments that physically model the same wave condition will have identical third-order velocity moments.

[34] Figure 5 (column 1, row b) clearly shows the differences in transport of fine sand between tunnel and flume experiments: In the tunnel, the transport direction reverses from onshore to offshore with increasing $<u_{red}^3>$. For the flume cases, the transport remains onshore. Figure 5 (column 2, row b) shows that these trends are reproduced by the model. Also, the moment of transition from onshore to offshore transport for fine sand ($<u_{red}^3> \approx 0.15$ m^3/s^3) is predicted correctly. Like in the experiments, the simulated transport rates of medium sized sand (Figure 5, row a) are also generally increasing with increasing $<u_{red}^3>$ (Figure 5, column 2, row b). The experimental results show both trends for larger (Figure 5, diamonds, measurements of *Dohmen-Janssen and Hanes* [2002]) as well as smaller (circles, [*Schretlen*, 2012])

net transport rates in wave flumes compared to tunnels (stars) for identical $<u_{red}^3>$. The accompanying model simulations (Figure 5, column 2, row a) can be represented well with one simple third-order power function $<q_s> = A <u_{red}^3>$. Again, this might be explained by a systematic difference between the two series of medium sand flume experiments, not reflected by the model, which results in generally smaller measured net transport rates in the experiments of *Schretlen* [2012] compared to *Dohmen-Janssen and Hanes* [2002]; a possible explanation is the sieve curve width. See *Schretlen* [2012] for further discussion of the experimental differences.

3.5. Sensitivity Analysis and Discussion

[35] We conclude the validation with a sensitivity analysis and discussion on the modeling concept. The sensitivity analysis focuses on model formulations for mixing, roughness, and hindered settling. Although the present choices for σ_t, k_N, and w_s find their basis in literature, their application for sheet-flow under waves is not without discussion. *Nielsen et al.* [2002], e.g., questioned the eddy diffusivity concept and found a settling velocity reduction significantly stronger than predicted by *Richardson and Zaki* [1954]. Next, some authors have suggested modeling flow over mobile beds using much larger k_N values [e.g., *Sumer et al.*, 1996; *Dohmen-Janssen and Hanes*, 2002] or used k_N as a d_{50} independent tuning parameter [*Ruessink et al.*, 2009]. In this study, we investigate the effect of decreasing/increasing σ_t, k_N, and p (hindered settling effect, equation (9a)) with a factor of about 1.5. In addition, we test for k_N increased one order of magnitude (test 5). The tests and results are presented in Figure 6 and Table 3.
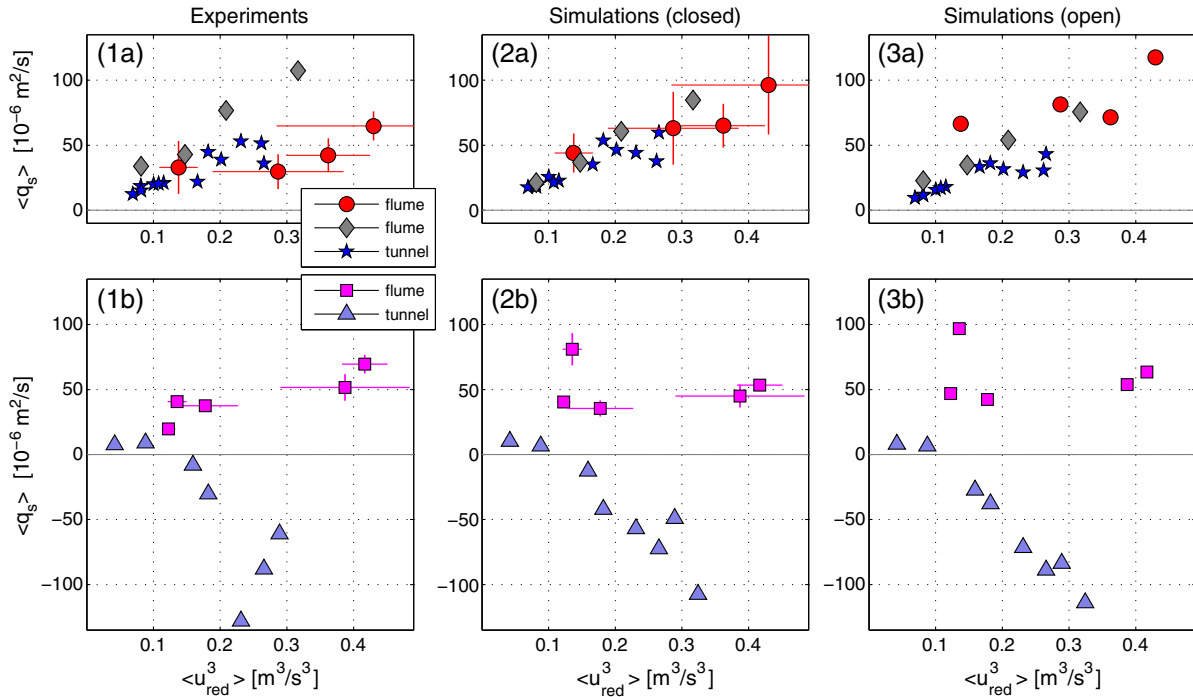
Figure 5. Measured (1a, 1b) and computed (2a, 2b) net sediment transport rates $<q_s>$ of medium (a) and fine (b) sands against the third-order velocity moment as determined from the oscillating part of the horizontal velocity u_{red}, for all conditions in Table 1. (3a, 3b) Results for simulations without compensation of mass transport in flume and tunnel (section 4.1).
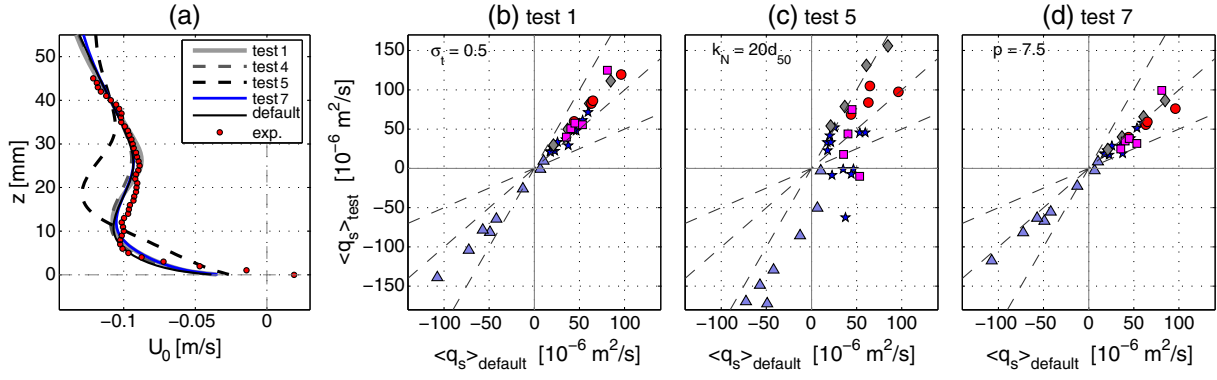
Figure 6. Results from the sensitivity analysis for a selection of tests from Table 3. (a) Measured and computed mean current velocity U_0; (b–d) transport rate $\langle q_s \rangle$ computed with adapted model parameter values against $\langle q_s \rangle$ computed with the original values, for all conditions of Table 1. (Default values: $\sigma_t = 0.7$, $k_N = 2d_{50}$, $p = 5.0$). Dashed lines: $y = \alpha x$, for α is 1/2, 1, and 2.

Table 3. Sensitivity Tests[a]

Set	Experiment	Default[b]	Test 1 $\sigma_t = 0.5$	Test 2 $\sigma_t = 1.0$	Test 3 $k_N = 1.3d_{50}$	Test 4 $k_N = 3d_{50}$	Test 5 $k_N = 20d_{50}$	Test 6 $p = 3.3$	Test 7 $p = 7.5$[c]
Flume medium	1–4	0.77	0.65	0.91	0.80	0.74	0.64	0.79	0.84
Flume fine	5–9	0.82	0.77	0.85	0.85	0.78	0.40	0.83	0.71
Flume medium	10–13	0.87	0.95	0.70	0.80	0.93	0.76	0.80	0.90
Tunnel medium	14–25	0.88	0.82	0.92	0.91	0.85	−0.50	0.90	0.85
Tunnel fine	26–33	0.80	0.63	0.61	0.79	0.72	0.23	0.69	0.56
All conditions	1–33	0.84	0.76	0.81	0.85	0.81	0.10	0.82	0.77

[a]Data reproduction quality measure $\langle S \rangle$ for all tests, both per set and total.
[b]Default model parameter choices: $\sigma_t = 0.7$; $k_N = 2.0d_{50}$; $p = 5.0$.
[c]A larger p leads to increased effects of hindered settling.

[36] First, we observe from Figure 6a that U_0 is only marginally affected by factor of 1.5 changes in σ_t, k_N, and p. However, the order of magnitude change in k_N (test 5) introduces a large overestimation of the level and magnitude of the maximum offshore boundary layer streaming. This results from increasing boundary layer thickness with increasing roughness, see also the model behavior tests in *Kranenburg et al.* [2012] (BL2-HYDRO). For a selection of tests, Figures 6b to 6d show $\langle q_s \rangle$ computed with adapted model parameters against $\langle q_s \rangle$ computed with the original values for the conditions of Table 1. By and large, test 1 (reduced σ_t, increased mixing) shows an increase of the absolute transport rates for all sets. In test 7 (increased p, increased hindered settling effect), the results for medium sized grains (Figure 6, circles, diamonds, stars) are nearly unaltered, whereas the fine sand cases (generally) show a slightly increased transport in offshore direction. Apparently, phase-lags effects increase in both tests, whereas the stronger mixing also strengthens the onshore transport mechanisms. The changes for $\langle q_s \rangle$ in test 5 (k_N increased with a factor 10) are clearly of another order of magnitude. Both for the sets with medium sand in a flume (Figure 6, circles, diamonds) and with fine sand in a tunnel (Figure 6, triangles), $|\langle q_s \rangle|$ increases drastically. The two other sets show completely scattered results, from an increase with a factor of 2 to a reversal of the transport direction. Table 3 lists the consequences for model-data comparison for all sensitivity tests. Clearly, from U_0 and $\langle q_s \rangle$ results, there is no need to adopt alternative formulations.

[37] A more fundamental question is whether it is justified to model sheet flow as sand in suspension. First, note that based on the nondimensional parameters θ and w_s/u_* in Table 1, all experimental conditions can be classified as well inside the domain of "suspension mode sheet flow" [*Wilson*, 1989: sheet flow for $\theta > 0.8$; *Sumer et al.*, 1996: suspension mode for $w_s/u_* < 0.8$–1.0). Also, regarding the classical distinction between bed load and suspended load, the Rouse number $P = w_s(\kappa u_*)^{-1}$ indicates that suspension load transport will dominate by far in most cases. Indeed, *Hassan and Ribberink* [2010], who used a suspension model with a bed-load formula to model the flux beneath $z = 2d_{50}$, found the bed-load component of minor importance for the total computed transport (except for their large grain test). Furthermore, although shifted to levels above $z = 0$ mm (instead of below $z = 0$, as measured in the pickup layer), the shape and magnitude of the net flux profiles also were reproduced very well. Apparently, the sheet-flow layer dynamics can to a certain extent be represented as an advection-diffusion process, with the present empirical model for reference concentration (neglecting the details of sediment entrainment and dynamics in concentrations close to the pack limit). Based on the validation results and the considerations above, we consider the suspension approach appropriate for the present research. More detailed investigation on erosion behavior and sheet-flow layer thickness would require further development and application of other modeling concepts, e.g., two-phase models.

4. Relative Importance of Various Free Surface Effects

[38] This section describes model simulations to investigate the relevance of the hydrodynamic differences between tunnel and flume experiments for sediment transport rates. We first study the role of contrasting return flow mechanisms in the two experimental settings (section 4.1). Subsequently, we focus on differences induced by advection processes inside the wave boundary layer. Their effects on sediment transport are illustrated with a discussion on velocities and concentrations beneath sinusoidal waves in section 4.2 and quantified for more realistic nonlinear waves in section 4.3.

4.1. Compensation of Mass Transport in Closed Tunnels and Flumes

[39] In a closed tunnel, the offshore wave shape streaming will cause an onshore-directed mass transport compensation current. The strength of this current not only depends on the streaming, but also on properties of the facility like height and width. Beneath progressive surface waves, the mass transport originates not only from wave shape streaming, but also from the onshore progressive wave streaming and especially the onshore Stokes drift. In a flume with closed ends, this will result in a mean pressure gradient driving an offshore-directed (Eulerian) compensating current. We determine the influence of these mass compensation
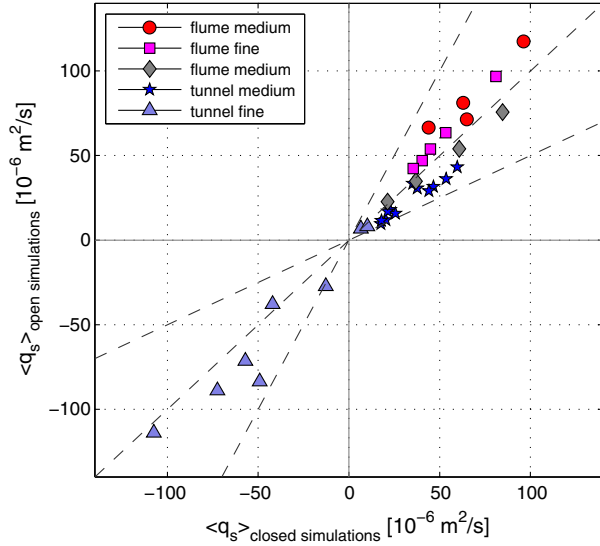
Figure 7. Computed net sediment transport rates $\langle q_s \rangle_{\text{open}}$ versus $\langle q_s \rangle_{\text{closed}}$; that is, simulations without the current that compensates the mass transport versus simulations with this current. Results for all conditions of Table 1. Dashed lines: $y = \alpha x$, for α is 1/2, 1, and 2.

mechanisms on sediment transport by comparing the earlier simulations with simulations of hypothetical open facilities, set up as described in section 2.2. Because the level z_{match} of the horizontal velocity measurements used before is practically outside the wave boundary for all used tunnel and flume experiments, we use u_{red} at $z = z_{\text{match}}$ as input signal to determine the oscillating horizontal pressure gradient. Figure 7 shows $\langle q_s \rangle$ for "open" versus "closed" simulations; Figure 5 (column 3, rows a and b) shows the newly computed $\langle q_s \rangle$ against $\langle u_{red}^3 \rangle$ (identical to $\langle u_{red}^3 \rangle$ for the measurements and closed simulations).

[40] As expected, Figure 7 shows that the return flow generally leads to less onshore transport for flume conditions (with offshore-directed return current) and to more onshore (or less offshore) transport for tunnel conditions (with onshore-directed return current). This influence of the return flow is generally not very large. Figure 5 (column 3, rows a and b) shows that the $\langle q_s \rangle$-$\langle u_{red}^3 \rangle$ trends are also not affected significantly. Compared to the closed simulations, the open simulations for medium sand show a more distinct trend for larger transport rates in flumes (both sets) compared to tunnels for identical $\langle u_{red}^3 \rangle$.

4.2. Advection Processes: Illustration for Sinusoidal Waves

[41] Next, we discuss one by one the additional free surface–related momentum and sediment advection processes in the horizontally nonuniform wave boundary layer, as present in flume and prototype situation and not in tunnels. These additional horizontal and vertical advection processes each appear in the reduced equations (1) or (8) in one single advective term (see Table 4). We illustrate the effects of these processes on boundary layer velocities and concentrations by comparing simulations with the advective terms one by one switched on to a reference simulation (REF) with all these terms switched off (BL1-model). All simulations are "open" simulations in which the model is forced with an identical sinusoidal horizontal free stream velocity with amplitude $\hat{u}_\infty = 1.0$ m/s and period $T = 6.5$ s. The simulations have been carried out for water depth $h = 3.5$ m and grain size $d_{50} = 0.1$ mm. The surplus of horizontal velocity and sediment concentration from the various free surface effects is shown in Figures 8a to 8d. Figures 8e and 8f show the vertical profile of the period-averaged sediment flux. The resulting net transport rates have been added to Table 4. Note that the reference simulation of a sinusoidal oscillating flow yields a zero wave-averaged velocity, sediment flux, and net transport rate.

[42] We first discuss $w\partial u/\partial z$. This single term is the driver of the additional onshore streaming under progressive waves. This occurs through a net downward transport of horizontal momentum into the boundary layer by the vertical orbital motion as a result of the phase shift of the horizontal

Table 4. Overview of Free Surface Effects (with sediment transport values matching Figure 8)

Nr	Physical Process	Mathematical Term	Primary Effect	Net Transport q_s (10^{-6} m²/s)	Current-Related Part (10^{-6} m²/s)
1	Vertical momentum advection	$w\partial u/\partial z$	Onshore streaming	38.3	40.0
2	Vertical sediment advection	$w\partial c/\partial z$	Adapted phase lag	9.0	0.9
3	Horizontal sediment advection	$u\partial c/\partial x$	Concentration modulation	50.0	0.1
4	Horizontal momentum advection	$u\partial u/\partial x$	Velocity skewness	9.6	2.6
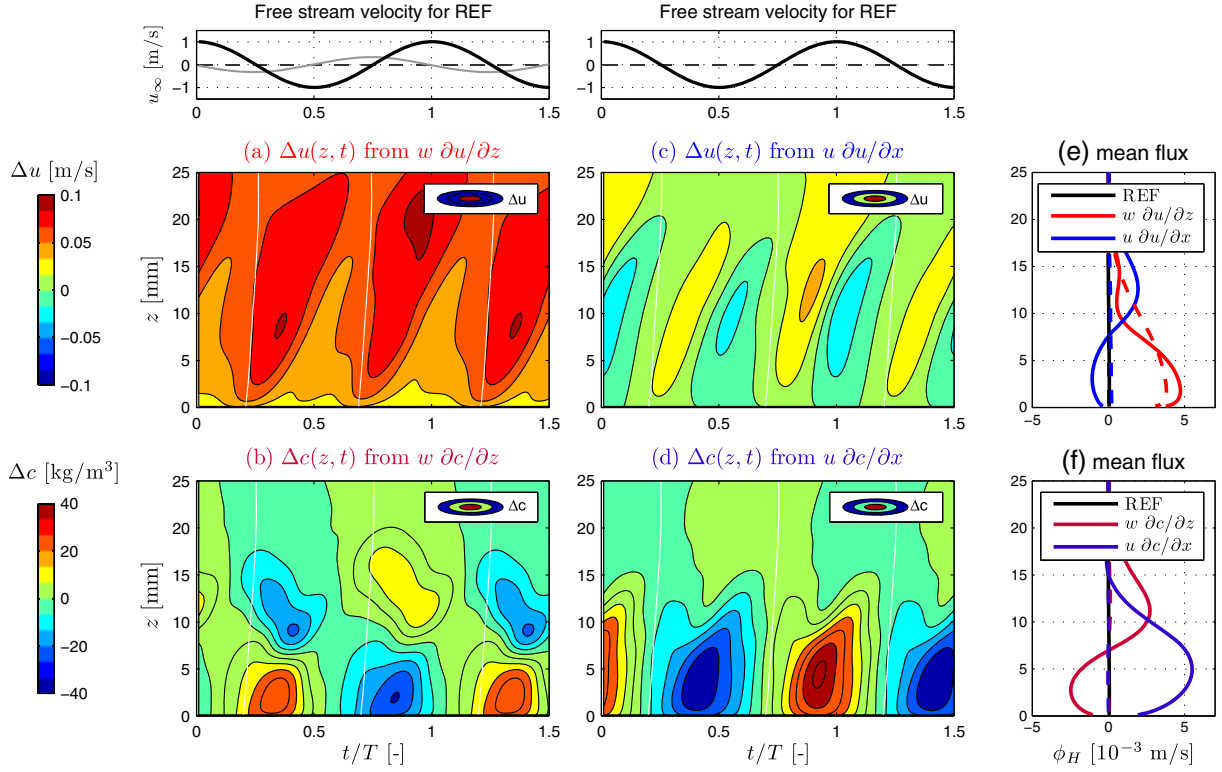
Figure 8. Surplus of horizontal velocity (a, c) or sediment concentration (b, d) induced by the various advective terms, with their consequence for the mean sediment flux (e, f). REF, reference simulation with all advective terms switched off. Solid lines represent total wave-averaged sediment flux $\overline{uc}$; dashed lines represent current-related sediment flux $\overline{u}\,\overline{c}$. Top panels show free stream velocities. White lines in (a–d) indicate flow reversal. Condition: sinusoidal wave with $T = 6.5$ s, $\hat{u}_\infty = 1.0$ m/s, $h = 3.5$ m, $d_{50} = 0.1$ mm.

orbital velocities over the boundary layer height. The extra onshore current in the wave boundary layer is clearly visible in the surplus velocities in Figure 8a. The primary effect of this current is an additional current-related (suspended) sediment flux over the whole wave boundary layer. The velocity skewness will also increase. Expected secondary effects are therefore increased pickup rates under the wave crest and stirring up of sediment to higher levels because of larger flow and turbulence intensities. Under the trough, the opposite will occur.

[43] The vertical orbital motion might also contribute to onshore transport trough vertical sediment advection. The vertical motion introduces a difference between the onshore and offshore phase of the wave: at the reversal of the flow from onshore to offshore, the orbital motion will be downward, whereas it will be upward during offshore to onshore flow reversal. This becomes relevant for the sediment concentration when grains are stirred up to levels where the vertical velocity $\widetilde{w}$ is on the order of the grain settling velocity w_s. In that case, the concentration at this level will decrease faster after the onshore movement and slower after the offshore movement. In other words, the phase-lag between velocity and concentration will behave differently under the wave crest and trough. Figure 8b shows the consequences of $w\partial c/\partial z$ for the concentration profiles: under the crest, more sediment is present at higher levels; under the trough, more sediment is present near the bed. Consequently, positive net sediment fluxes appear higher up in the boundary layer, and negative net sediment fluxes appear

near the bed. These opposite contributions finally lead to a relatively small influence of vertical sediment advection on the vertically integrated net flux or net transport rate.

[44] Next, in the horizontally nonuniform flow field, the advection of sediment by the horizontal orbital motion might also contribute to onshore transport. The horizontal gradients in the sediment flux cause an accumulation of sediment in front of the wave top, where the flux gradient $\partial(uc)/\partial x < 0$. Behind the top, the opposite occurs. As a result, the absolute rates of change of the sediment concentration are larger and the concentration reacts faster on velocity changes during onshore flow than during offshore flow. A modulation in the concentration takes place, with an amplification of the concentration peak at maximum onshore velocity and a reduction at maximum offshore velocity (see Figure 8d). This induces a net contribution to sediment transport in the onshore direction. An analytical illustration of this process is given in Appendix A (considering horizontal sediment exchange only). It shows that the additional net flux due to the modulation is proportional to $\hat{u}^2/c_p$. Note that $\hat{u}/c_p$ denotes the order of magnitude of the advective terms compared to the other terms, and that the advection terms $w\partial c/\partial z$ and $u\partial c/\partial x$ together describe Stokes's drift of sand in an Eulerian model.

[45] Like the effect of $u\partial c/\partial x$ for sediment, the primary effect of $u\partial u/\partial x$ is a modulation of the horizontal orbital velocities. When forced with a sinusoidal pressure gradient, $u\partial u/\partial x$ would lead to an increased horizontal velocity under the wave top and a decreased velocity under the wave trough (i.e., velocity skewness). However, here we forced the

model to match a sinusoidal free stream velocity. As a result, the nonlinear term induces slightly acceleration-skewed flow inside the boundary layer (increased acceleration, decreased deceleration). The resulting difference in turbulence yields sediment stirring to higher (less high) levels during onshore (offshore) flow, which yields small positive net sediment fluxes at higher levels (see Figures 8c and 8e).

[46] The primary effects of the various advection processes beneath progressive waves are summarized in Table 4. Especially $w\partial u/\partial z$ and $u\partial c/\partial x$ have a clear onshore influence on net transport rates trough onshore contribution to the net sediment flux over the entire vertical. The other two terms ($w\partial c/\partial z$ and $u\partial u/\partial x$) lead to both onshore (higher up in the vertical) and offshore fluxes (at lower levels). This results (for these conditions) in only small effects on the net sediment transport. It is also shown that the contribution from $u\partial c/\partial x$ to the net flux is nearly entirely wave related ($< \widetilde{u}\widetilde{c} >$), whereas the contribution from $w\partial u/\partial z$ (streaming) is mostly current related ($<u><c>$). Finally, the advection of turbulence properties (terms 2 and 3 of equations (4) and (5)) has only a marginal effect on the sediment flux profile and is not further discussed.

4.3. Advection Processes: Tests for Realistic Waves

[47] Where the effects of the various advection processes on velocities and concentrations were illustrated for sinusoidal waves in section 4.2, we now investigate their relevance for sediment transport for more realistic nonlinear wave conditions. For that, we define a number of test conditions with constant wave period T and water depth h, but gradually increasing wave height H. From T, h, and H, we determine the fluctuating part of the near bed free stream horizontal velocity $\tilde{u}_\infty(t)$ with the Fourier approximation method of *Rienecker and Fenton* [1981]. This results in velocity signals with increasing velocity skewness for increasing H. Using the method of *Rienecker and Fenton* [1981], acceleration skewness from steepening of the wave toward breaking is not considered. Seaward of the surf zone, we consider this a justified approach, based on indications that waves in that region are predominantly velocity skewed [*Ruessink et al.*, 2009]. An overview of the test conditions is given in Table 5. Next to wave height H, the table gives the amplitudes of four harmonic components of $\tilde{u}_\infty$, namely $\hat{u}_{\infty,1-4}$, together with velocity skewness measures $R = \tilde{u}_{\infty,crest}/(\tilde{u}_{\infty,crest} - \tilde{u}_{\infty,trough})$ and $Sk_u = \overline{\tilde{u}_\infty^3}/\left(\overline{\tilde{u}_\infty^2}\right)^{1.5}$, energy measure $u_{rms} = \sqrt{\overline{\tilde{u}_\infty^2}}$, and

the third-order velocity moment $< \tilde{u}_\infty^3 >$, all determined from $\tilde{u}_\infty$. This free stream velocity $\tilde{u}_\infty$ is used to force the model; the mean velocity is allowed to develop freely (open simulation).

[48] For the defined test cases, the sediment transport has been simulated with all advective terms switched on (FLU, because it models the flume situation), with all advective terms switched off (REF), and with only $w\partial u/\partial z$, $w\partial c/\partial z$, $u\partial c/\partial x$, or $u\partial u/\partial x$ switched on individually. This has been done for both medium sized sand ($d_{50} = 0.25$ mm) and fine sized sediment ($d_{50} = 0.14$ mm). The computed transport rates are shown in Figure 9, plotted against the third-order velocity moment. For the fine grains, the percentage of the difference in transport between FLU and REF covered by a single advection term has been added to Table 5, where TERM (%) = $(q_{s,\text{TERM}} - q_{s,\text{REF}})/(q_{s,\text{FLU}} - q_{s,\text{REF}})$.

[49] The computed transport rates provide insight in the relative importance of individual advective processes in explaining the differences between tunnels and flumes, and show how the relative contribution of the various terms changes with changing wave and bed conditions. We learn from Figure 9 that progressive wave streaming, induced by $w\partial u/\partial z$, indeed contributes substantially to onshore sediment transport. For the medium grains, almost the complete difference between flume (FLU) and tunnel (REF) simulations is covered with vertical momentum advection taken into account. However, in the case of fine sand, with higher volumes of sediment in suspension, also the gradients in horizontal advection become important, especially $u\partial c/\partial x$. Table 5 shows that the relative contribution of this term also increases with increasing wave height. For the wave and bed conditions from the realistic ranges investigated in this study, the effect of $w\partial c/\partial z$ turns out to be negligible. Finally, note that the sum of the four separate contributions is smaller than but close to 100% for the least energetic and just over 100% for the most energetic condition. This means that the interaction between the various advective processes is small.

5. Discussion

### 5.1. Relevance for Sediment Transport Formulas

[50] We have shown that both progressive wave streaming and gradients in horizontal advection are free surface effects that can contribute significantly to sediment transport beneath waves. Therefore, we believe that these free surface effects should be accounted for in sediment

Table 5. Overview of Test Conditions,[a] With Relative Contribution of Individual Advective Terms to the Total Sediment Transport[b]

H (m)	$\hat{u}_{\infty,1}$ (m/s)	$\hat{u}_{\infty,2}$ (m/s)	$\hat{u}_{\infty,3}$ (m/s)	$\hat{u}_{\infty,4}$ (m/s)	R (-)	Sk_u (-)	u_{rms} (m/s)	$<\tilde{u}_\infty>^3$ (m³/s³)	$w\partial u/\partial z$ (%)	$w\partial c/\partial z$ (%)	$u\partial c/\partial x$ (%)	$u\partial u/\partial x$ (%)
0.7	0.50	0.08	0.01	—	0.58	0.34	0.36	0.016	96	0	5	−4
0.8	0.56	0.10	0.01	—	0.59	0.38	0.41	0.025	90	1	7	−3
0.9	0.62	0.13	0.02	—	0.60	0.43	0.45	0.040	83	2	11	−0
1.0	0.68	0.15	0.02	—	0.61	0.47	0.50	0.057	76	3	14	3
1.1	0.74	0.18	0.03	0.01	0.62	0.51	0.54	0.080	70	4	16	7
1.2	0.79	0.21	0.04	0.01	0.63	0.55	0.58	0.107	65	5	19	10
1.3	0.84	0.24	0.05	0.01	0.64	0.59	0.62	0.139	61	6	21	14
1.4	0.89	0.27	0.06	0.01	0.65	0.63	0.66	0.182	58	7	23	17
1.5	0.93	0.30	0.07	0.01	0.65	0.67	0.69	0.222	56	8	25	20
1.6	0.97	0.33	0.08	0.01	0.66	0.71	0.73	0.272	54	8	27	22

[a]T = 6.5 s and h = 3.5 m in all tests.
[b]For the fine sand tests, with d_{50} = 0.14 mm.
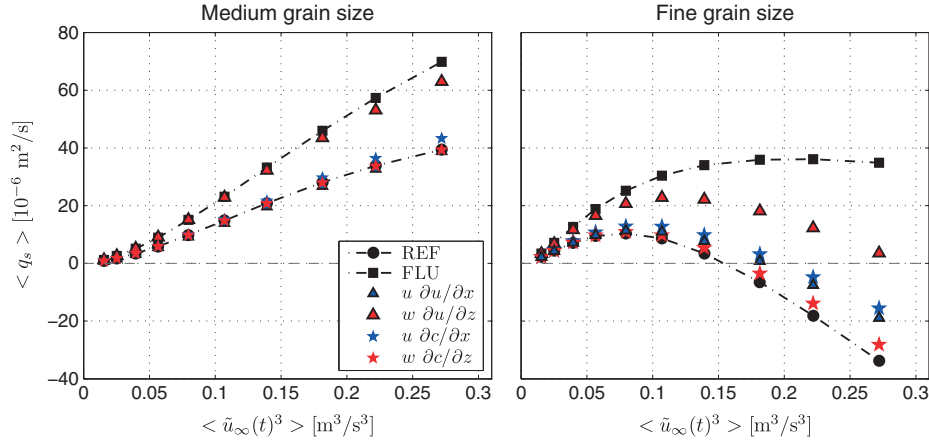
Figure 9. Net transpowrt rates $<q_s>$ of medium (0.25 mm) and fine (0.14 mm) sized sediments for the wave conditions of Table 5, plotted against $<\tilde{u}_\infty^3>$. Results obtained with all advective terms switched on (FLU), all advective terms switched off (REF), and only $w\partial u/\partial z$, $w\partial c/\partial z$, $u\partial c/\partial x$, or $u\partial u/\partial x$ switched on are shown.

transport formulas. This is generally not the case in transport formulas used in present-day morphodynamic modeling, developed and calibrated from tunnel experiments [see, e.g., *Davies et al.*, 2002]. Sediment transport formulas predict the transport from the free stream velocity or bed shear stress. "Quasi-steady" formulas directly relate the instantaneous transport to the instantaneous velocity or stress through power laws and empirical coefficients [e.g., *Bailard*, 1981; *Ribberink*, 1998]. "Semi-unsteady" formulas account for phase-lag effects through inclusion of a phase-lag parameter representing the ratio of sediment settling time and wave period [e.g., *Dibajnia and Watanabe*, 1998; *Dohmen-Janssen et al.*, 2002]. The first to account for progressive wave streaming in transport formulas were *Nielsen* [2006] and *Van Rijn* [2007]. They compute the transport with either an extra onshore wave-averaged (free stream) velocity [*Van Rijn*, 2007] or bed shear stress [*Nielsen*, 2006] added to the oscillatory input of their transport formula. Note that new parameterizations for this additional mean velocity and stress are provided by *Kranenburg et al.* [2012]. The effect of horizontal (sediment) advection gradients was not included, or it was assumed to be strongly correlated to the streaming effect [*Nielsen*, 2006]. This study's differentiation between the various free surface effects shows that the relative contribution is strongly grain size dependent. Here we present a parameterization for the horizontal advection effects consistent with the insights from this study.

[51] First, consider a simple transport formula that expresses the depth-integrated sediment flux q_s as function of the free stream velocity u_∞ and the depth-averaged volume concentration $C(t)$:

$$q_s(t) = \int_{z=zbed}^{zbed+\delta} ucdz = \alpha\delta u_\infty(t)C(t) \quad (19)$$

with δ is the thickness of the layer over which transport (and averaging) takes place, and α a distribution coefficient related to the shape of the concentration and velocity profiles [O(1)]. Second, note that the time-dependent behavior of the depth-averaged concentration $C(t)$ in gradually

varying flows can be represented in a schematic way by a relaxation equation:

$$\frac{\partial C(t)}{\partial t} = \frac{\gamma\{C_{eq}(t) - C(t)\}}{T_a} \quad (20)$$

[see *Galappatti and Vreugdenhil*, 1985]. In this relaxation equation, T_a is the time scale of adaptation of the sediment concentration to the equilibrium concentration C_{eq}, and γ is a coefficient related to the shape of the concentration profile. The (depth-averaged) C_{eq} reflects the "carrying capacity" of the flow; that is, the concentration for which the sediment settling and pickup are equal. C_{eq} is directly related to the instantaneous forcing through the Shields number θ [see, e.g., *Van Rijn*, 1993]. Here, we apply $C_{eq}(t) = \beta\theta(t)$, with β a coefficient. The key element of the parameterization is the expression for T_a. Starting from the advection-diffusion equation, we derive in Appendix B that the advection effects in horizontally nonuniform flow can be included in the concentration equation (20) and transport formula (19) with

$$T_a(t) = \frac{\delta}{w_s}\left\{1 - \frac{\alpha u_\infty(t)}{c_p}\right\} \quad (21)$$

where c_p is the wave propagation speed, and $\{1 - \alpha u_\infty/c_p\}$ is <1 during onshore flow and >1 during offshore flow. Note that in oscillatory flows, T_a reduces to δ/w_s. This is the settling time used also by *Dohmen-Janssen et al.* [2002] in the phase-lag parameter T_a/T for the semi-unsteady description of fine sand transport in tunnels. Hereby δ is the particle entrainment height (also an appropriate measure for the transport layer thickness), and w_s is the settling velocity. Next, for medium to coarse sand, δ/w_s will be small. In that case, equation (20) yields concentrations immediately adapting to changes in the forcing, and sediment transport formula (19) becomes quasi-steady. With the full equation for T_a, the main features of the advection effects under progressive waves are represented: (1) The concentration will adapt faster during the onshore motion than during the offshore
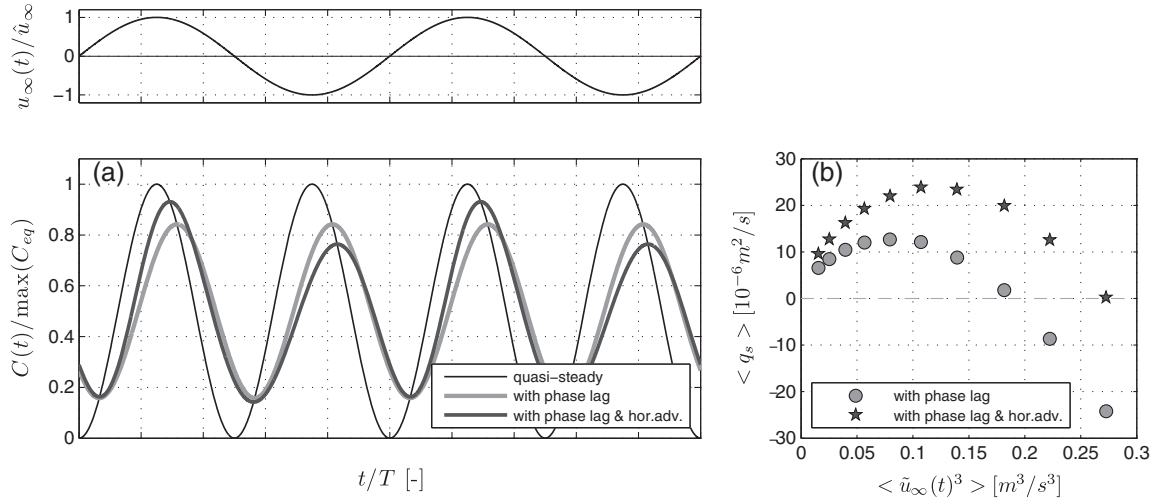
Figure 10. (a) Depth-averaged concentration C beneath a sinusoidal wave (upper panel), respectively, with a quasi-steady approach (thin black line), with phase-lag effects after *Dohmen-Janssen et al.* [2002] (thick light gray line), and with phase-lag in combination with horizontal advection effects (dark gray line, T_a according to equation (21)). (b) Period-averaged sediment transport $<q_s>$ for the cases of Table 5 computed using T_a both with and without effects of horizontal advection. Parameters case (a): $T = 6.5$ s, $\hat{u}_\infty = 1.2$ m/s, $h = 3.0$ m, $d_{50} = 0.14$ mm; used coefficients: $\alpha = 2.0$, $\beta = 0.01$, $\gamma = 10$.

motion, (2) increased/decreased maximum concentration will be found under the wave crest/trough, and (3) the advection effects will increase with decreasing grain size.

[52] We illustrate the behavior of the parameterization with Figure 10. Figure 10a shows the concentration beneath a sinusoidal wave computed from relaxation equation (20), respectively, with a quasi-steady approach ($T_a = 0$), with phase-lag effects ($T_a = \delta/w_s$), and with phase-lag effects beneath progressive waves, i.e., with T_a from equation (21). Comparison with Figure 8d shows that the latter yields concentration behavior consistent with the numerical model results. Next, Figure 10b shows, for the cases of Table 5, that also the numerically computed $<q_s>$ can be reproduced well using equations (19–21). In these calculations, we set the transport layer thickness to 10 times the sheet-flow layer thickness: $\delta = 10\delta_s$. From *Dohmen-Janssen et al.* [2002], we use $\delta_s = 35d_{50}\theta_{max}$. The maximum Shields parameter is $\theta_{max} = 1/2f_wu_{max}^2/(\Delta gd_{50})$. We computed f_w following *Swart* [1974] with bed roughness height $k_N = 2d_{50}$. Settling velocity w_s is computed from equation (9b). Coefficients α, β, and γ were used as calibration parameters tuning the balance between the processes. Note that the effects of horizontal sediment and momentum advection are strongly correlated (Figure 9; Table 5). Therefore, parameter T_a can be applied to account for both advection processes together.

[53] Considering the flume measurements of transport of fine sand under velocity-skewed waves (Figure 5b), one may wonder whether there is any need to let transport formulas evolve further away from the simple quasi-steady approach. After all, the correlation between $<q_s>$ and $<u_{red}^3>$ for these cases is very strong. One should realize that, in these cases, the offshore transport from phase-lag effects, so important in velocity-skewed oscillatory tunnel flow over fine sand, and the onshore transport from

advection effects nearly completely cancel each other out. These processes will not always (counter)act in the same balance. For instance, when a velocity-skewed wave becomes steeper, the onshore contribution from advection effects remains, whereas the offshore contribution due to phase-lag effects decreases. (For purely acceleration-skewed waves, phase-lag effects even contribute to onshore transport [*Van der A*, 2010].) We therefore believe that both processes should be considered in parameterized transport formulas.

5.2. Limitations of This Study

[54] Both in the model formulation and validation, this study is limited to the suspension-mode sheet-flow regime. The numerical tests to capture the various advection effects were carried out for a parameter range extending beyond this regime. Herein, we neglect that actually ripples may be expected beneath the lowest energy waves of Table 5 (Shields number $\theta < 0.8$). The effects of streaming and horizontal advection on net transport rates over rippled beds, with more complicated flow patterns, are still unknown and need further research. Other issues not considered in this study are the relevance for sediment transport of bed-level variation and spreading in grain size. The potential role of the sieve curve width for the transport rates observed by *Schretlen* [2012] may initiate further research here on.

6. Conclusions

[55] A numerical model has been developed to investigate the influence of free surface effects on transport of sediment in the wave boundary layer beneath regular progressive waves. The 1DV Reynolds averaged Navier-Stokes boundary layer model with an advection-diffusion formulation for sediment concentration and a k-ε turbulence closure with feedback of sediment on the flow-through stratification

effects has been successfully validated with recent full-scale flume measurements on both boundary layer flow and suspension mode sheet-flow sediment transport under velocity-skewed waves. The validation showed that progressive wave streaming and stratification effects are essential processes to reproduce measured wave-averaged current profiles. As with the transport measurements, the model results show a reversal from offshore to onshore wave-averaged transport of fine sediment under influence of the free surface effects. It was subsequently investigated to what extent the increased onshore transport could be attributed to progressive wave streaming. We conclude that this onshore streaming indeed contributes largely to increased onshore transport rates in flumes compared to tunnels. However, especially for fine grains, other free surface effects also are important. In particular, gradients in horizontal advection of sediment in the nonuniform flow-field beneath surface waves are found to influence fine sand transport significantly. This mechanism amplifies respectively reduces the maximum concentration during onshore respectively offshore motion, causing increased onshore transport rates. Therefore, we conclude that, next to streaming, also the latter should be considered in formulas of wave-induced sediment transport in morphodynamic modeling. It is proposed to incorporate this process through a phase-lag parameter with a wave-phase–dependent adaptation time T_a for sediment concentration in unsteady flow. The proposed parameter T_a, given in equation (21) covers the relevant characteristics of the physical process, yields transport rates comparable to the numerical model, and is therefore a suitable parameterization to be included in practical sand transport formulas.

Appendix A: Analytical Illustration of the Effect of Horizontal Sediment Advection

[56] The contribution of intrawave gradients in horizontal advection to sediment transport in the direction of wave propagation can be analytically illustrated as follows: Moving with the wave propagation speed c_p, the material derivative of a steady harmonic oscillation is zero for all quantities (equation (10)), including the sediment flux $f = \tilde{u}c$:

$$\frac{\partial f}{\partial t} + c_p \frac{\partial f}{\partial x} = 0 \tag{A1}$$

[57] We substitute this equality into the sediment balance, neglecting all vertical sediment exchange:

$$\frac{\partial c}{\partial t} + \frac{\partial \tilde{u}c}{\partial x} = \frac{\partial}{ct}\left\{c - \frac{\tilde{u}c}{c_p}\right\} = 0 \tag{A2}$$

[58] By integration, an expression for c can be derived showing the variation of c with $\tilde{u}$. Taylor expansion around $\tilde{u}/c_p \approx 0$ yields an approximation valid for $\tilde{u}/c_p \ll 1$ (α is the integration constant):

$$c(x,t) = \alpha\left(1 - \frac{\tilde{u}(x,t)}{c_p}\right)^{-1} \approx \alpha\left(1 + \frac{\tilde{u}(x,t)}{c_p}\right) \tag{A3}$$

[59] Multiplication with $\tilde{u}$ gives an expression for the flux f that shows the onshore contribution to period-averaged sediment transport:

$$f(x,t) \approx \alpha\tilde{u} + \frac{\alpha\tilde{u}^2}{c_p} \to \bar{f} \approx \frac{\alpha\hat{u}^2}{2c_p} \tag{A4}$$

Appendix B: Derivation of T_a, Time Scale of Adaptation

[60] The proposed time scale T_a to include the effects of horizontal gradients in sediment advection has been derived from the advection-diffusion equation for sediment:

$$c_t + (uc)_x + (wc)_z = (w_s c + \varepsilon c_z)_z \tag{B1}$$

where subscripts t, x, and z denote derivatives. The vertical sediment flux φ being:

$$\varphi = -\{(w_s - w)c + \varepsilon c_z\} \tag{B2}$$

the sediment balance can be written as

$$c_t + (uc)_x = -\varphi_z \tag{B3}$$

[61] We integrate this expression from the bottom $z = 0$ to a constant level in the wave boundary layer $z = \delta$ where the sediment concentration (and vertical flux) become negligible (e.g., the maximum stirring height or 10 times the sheet-flow layer thickness). Subsequently, we shift integration and differentiation, and divide all terms by thickness δ to obtain

$$C_t + (\overline{uc})_x = \frac{\varphi(0)}{\delta} \tag{B4}$$

where capital and over bar denote depth averaging. u and c are not uniformly distributed over the vertical. Using a distribution coefficient α, we express the second term in the free stream velocity u_∞ and the depth-averaged concentration C, such that $\overline{uc} = \alpha u_\infty C$. With this approach, we follow the approximation of *Galappatti and Vreugdenhil* [1985] for shallow, gradually varying flows. Next, we split up the second term in equation (B4) into two separate derivatives:

$$(\alpha u_\infty C)_x = \alpha u_\infty (C)_x + \alpha C(u_\infty)_x \tag{B5}$$

[62] The first is subsequently rewritten using the transformation $\frac{\partial}{\partial x} = -\frac{1}{c_p}\frac{\partial}{\partial t}$ for uniform waves (with c_p the propagation speed of the wave). The second term is rewritten assuming a constant ratio ξ between free stream velocity u_∞ and depth-averaged velocity U, and using flow continuity over the transport layer:

$$\frac{\partial u_\infty}{\partial x} = \frac{\partial \xi U}{\partial x} = \xi\frac{\partial U}{\partial x} = -\xi\frac{w(\delta)}{\delta} \tag{B6}$$

[63] As a result, we can write equation (B4) as

$$\left\{1 - \frac{\alpha u_\infty}{c_p}\right\}C_t - \alpha\xi C\frac{w(\delta)}{\delta} = \frac{\varphi(0)}{\delta} \qquad (B7)$$

[64] The vertical sediment flux φ at the bottom is the net result of pickup and deposition: $\varphi(0) = p_{up} - dep$, with p_{up} a function of the instantaneous bed shear stress and dep the result of vertical settling of sand near the bed. With the near bed concentration c_{bed} related to the depth-averaged concentration C through a shape coefficient $\gamma \gg 1$, $dep = w_s c_{bed} = w_s\gamma C$. Substitution into equation (B7) gives

$$\left\{1 - \frac{\alpha u_\infty}{c_p}\right\}C_t = \frac{1}{\delta}\left\{p_{up} - w_s\gamma C + \alpha\xi Cw(\delta)\right\} \qquad (B8)$$

[65] The vertical orbital velocities in the wave boundary layer are generally smaller or of the same order of magnitude as the sand settling velocity, i.e., $w(\delta) \leq w_s$. Next, α and ξ are of order O(1), so that $\gamma \gg (\alpha\xi)$. Therefore, the third term on the right-hand side of equation (B8) can be neglected in comparison with the second term. This results in the relaxation expression:

$$C_t = \frac{\frac{\gamma w_s}{\delta}\left\{\frac{p_{up}}{\gamma w_s} - C\right\}}{\left\{1 - \frac{\alpha u_\infty}{c_p}\right\}}; \qquad \text{or} \qquad C_t = \frac{\gamma(C_{eq} - C)}{T_a} \qquad (B9)$$

with

$$C_{eq} = \frac{p_{up}}{\gamma w_s}; \qquad \text{and} \qquad T_a = \frac{\delta}{w_s}\left\{1 - \frac{\alpha u_\infty}{c_p}\right\} \qquad (B10)$$

References

Amoudry, L., T.-J. Hsu, and P. L.-F. Liu (2008), Two-phase model for sand transport in sheet flow regime, *J. Geophys. Res.*, *113*(C3), 1–15, doi:10.1029/2007JC004179.

Bailard, J. A. (1981), An energetics total load sediment transport model for a plane sloping beach, *J. Geophys. Res.*, *86*(C11), 10,938–10,954.

Blondeaux, P., G. Vittori, A. Bruschi, F. Lalli, and V. Pesarino (2012), Steady streaming and sediment transport at the bottom of sea waves, *J. Fluid Mech.*, *697*, 115–149, doi:10.1017/jfm.2012.50.

Breugem, A. (2012), Transport of suspended particles in turbulent open channel flows, PhD thesis, Delft University of Technology, Netherlands.

Conley, D. C., S. Falchetti, I. P. Lohmann, and M. Brocchini (2008), The effects of flow stratification by non-cohesive sediment on transport in high-energy wave-driven flows, *J. Fluid Mech.*, *610*, 43–67, doi:10.1017/S0022112008002565.

Davies, A. G., L. C. V. Rijn, J. S. Damgaard, J. V. D. Graaff, and J. S. Ribberink (2002), Intercomparison of research and practical sand transport models, *Coastal Eng.*, *46*, 1–23.

Dibajnia, M., and A. Watanabe (1998), Transport rate under irregular sheet flow conditions [online], *Coastal Eng.*, *35*(3), 167–183, doi:10.1016/

S0378-3839(98)00034-9. [Available at: http://linkinghub.elsevier.com/retrieve/pii/S0378383998000349].

Dohmen-Janssen, C. M., and D. M. Hanes (2002), Sheet flow dynamics under monochromatic nonbreaking waves, *J. Geophys. Res.*, *107*(C10), 1–21, doi:10.1029/2001JC001045.

Dohmen-Janssen, C. M., D. F. Kroekenstoel, W. N. Hassan, and J. S. Ribberink (2002), Phase lags in oscillatory sheet flow: Experiments and bed load modelling, *Coastal Eng.*, *46*(1), 61–87, doi:10.1016/S0378-3839(02)00056-X.

Fuhrman, D. R., J. Fredsøe, and B. M. Sumer (2009), Bed slope effects on turbulent wave boundary layers: 2. Comparison with skewness, asymmetry, and other effects, *J. Geophys. Res.*, *114*(C3), 1–19, doi:10.1029/2008JC005053.

Galappatti, G., and C. B. Vreugdenhil (1985), A depth-integrated model for suspended sediment transport, *J. Hydraulic Res.*, *23*(4), 359–377.

Gonzalez Rodriquez, D. (2009), Wave boundary layer hydrodynamics and cross-shore sediment transport in the surf zone, PhD thesis, Massachusetts Insitute of Technology, Cambridge, Mass.

Hassan, W. N. M., and J. S. Ribberink (2010), Modelling of sand transport under wave-generated sheet flows with a RANS diffusion model, *Coastal Eng.*, *57*(1), 19–29, doi:10.1016/j.coastaleng.2009.08.009.

Henderson, S. M., J. S. Allen, and P. A. Newberger (2004), Nearshore sandbar migration predicted by an eddy-diffusive boundary layer model, *J. Geophys. Res.*, *109*(C6), 1–15, doi:10.1029/2003JC002137.

Holmedal, L. E., and D. Myrhaug (2009), Wave-induced steady streaming, mass transport and net sediment transport in rough turbulent ocean bottom boundary layers, *Cont. Shelf Res.*, *29*(7), 911–926, doi:10.1016/j.csr.2009.01.012.

Hsu, T.-J., S. Elgar, and R. T. Guza (2006), Wave-induced sediment transport and onshore sandbar migration, *Coastal Eng.*, *53*(10), 817–824, doi:10.1016/j.coastaleng.2006.04.003.

Kranenburg, W. M., J. S. Ribberink, R. E. Uittenbogaard, and S. J. M. H. Hulscher (2012), Net currents in the wave bottom boundary layer: On wave shape streaming and progressive wave streaming, *J. Geophys. Res.*, *117*, F03005, doi:10.1029/2011JF002070.

Longuet-Higgins, M. S. (1953), Mass transport in water waves, *Philos. Trans. R. Soc. London, Ser. A*, *245*(903), 535–581.

Nielsen, P., K. V. D. Wal, and L. Gillan (2002), Vertical fluxes of sediment in oscillatory sheet flow, *Coastal Eng.*, *45*, 61–68.

Nielsen, P. (2006), Sheet flow sediment transport under waves with acceleration skewness and boundary layer streaming, *Coastal Eng.*, *53*(9), 749–758, doi:10.1016/j.coastaleng.2006.03.006.

O'Donoghue, T., and S. Wright (2004), Flow tunnel measurements of velocities and sand flux in oscillatory sheet flow for well-sorted and graded sands, *Coastal Eng.*, *51*(11–12), 1163–1184, doi:10.1016/j.coastaleng.2004.08.001.

Ribberink, J. S. (1998), Bed-load transport for steady flows and unsteady oscillatory flows, *Coastal Eng.*, *34*, 59–82.

Ribberink, J. S., and A. A. Al-Salem (1994), Sediment transport in oscillatory boundary layers in cases of rippled beds and sheet flow, *J. Geophys. Res.*, *99*(C6), 12,707–12,727.

Ribberink, J. S., and A. A. Al-Salem (1995), Sheet flow and suspension of sand in oscillatory boundary layers, *Coastal Eng.*, *25*(3–4), 205–225, doi:10.1016/0378-3839(95)00003-T.

Ribberink, J. S., and Z. Chen (1993), Sediment transport of fine sand under asymmetric oscillatory flow, Delft Hydraulics, Delft, The Netherlands.

Ribberink, J. S., J. J. van der Werf, T. O'Donoghue, and W. N. M. Hassan (2008), Sand motion induced by oscillatory flows: Sheet flow and vortex ripples, *J Turbulence*, *9*(20), 1–32, doi:10.1080/14685240802220009.

Richardson, J. F., and W. N. Zaki (1954), Sedimentation and fluidisation: Part I, *Trans. Inst. of Chemical Eng.*, *32*, S82–S100, doi:10.1016/S0263-8762(97)80006-8.

Rienecker, M. M., and J. D. Fenton (1981), A Fourier approximation method for steady water waves, *J. Fluid Mech.*, *104*, 119–137.

Rodi, W. (1984), Turbulence Models and Their Applications in Hydraulics. A State of the Art Review, 2nd ed., IAHR, Delft, Netherlands.

Ruessink, B. G., T. J. J. van den Berg, and L. C. van Rijn (2009), Modeling sediment transport beneath skewed asymmetric waves above a plane bed, *J. Geophys. Res.*, *114*(C11), 1–14, doi:10.1029/2009JC005416.

Schretlen, J. L. M. (2012), Sand transport under full-scale progressive surface waves, PhD thesis, University of Twente, Enschede, Netherlands. [Available at: http://doc.utwente.nl/80884.]

Schretlen, J. L. M., J. S. Ribberink, and T. O'Donoghue (2011), Boundary layer flow and sand transport, in Proceedings of 32nd International Conference on Coastal Engineering, edited by J. McKee Smith and P. Lynett, pp. 1–14, CERC, Shanghai, China, doi:10.9753/icce.v32.sediment.4.

Sumer, B. M., A. Kozakiewicz, J. Fredsoe, and R. Deigaard (1996), Velocity and concentration profiles in sheet-flow layer of movable bed, *J. Hydraulic Eng.*, *122*(10), 549–558.

Swart, D. H. (1974), Offshore Sediment Transport and Equilibrium Beach Profiles, Delft Hydraulics Laboratory Publ. no. 131, Delft, Netherlands.

Trowbridge, J., and O. S. Madsen (1984), Turbulent wave boundary layers 2. Second-order theory and mass transport, *J. Geophys. Res.*, *89*(C5), 7999–8007.

Uittenbogaard, R. E., J. Bosboom, and T. Van Kessel (2001), *Numerical Simulation of Wave-Current Driven Sand Transport: Theoretical Background of the beta-Release of the POINT-SAND Model*, Report Z2899.10, Delft Hydraulics, Delft, The Netherlands.

Van der A, D. A. (2010), Effects of acceleration skewness on oscillatory boundary layers and sheet flow sand transport, PhD thesis, University of Aberdeen, Aberdeen, U. K.

Van der A, D. A., T. O'Donoghue, A. G. Davies, and J. S. Ribberink (2011), Experimental study of the turbulent boundary layer in acceleration-skewed oscillatory flow, *J. Fluid Mech.*, *684*, 251–283, doi:10.1017/jfm.2011.300.

Van Rijn, L. C. (1993), Principles of Sediment Transport in Rivers, Estuaries and Coastal Seas, Aqua Publications, Amsterdam, Netherlands.

Van Rijn, L. C. (2007), Unified view of sediment transport by currents and waves. I: Initiation of motion, bed roughness, and bed-load transport, *J. Hydraulic Eng.*, *133*(6), 649, doi:10.1061/(ASCE)0733-9429(2007) 133:6(649).

Wilson, K. C. (1989), Friction of wave-induced sheet flow, *Coastal Eng.*, *12*, 371–379.

Winterwerp, J. C. (2001), Stratification effects by cohesive and noncohesive sediment, *J. Geophys. Res.*, *106*(C10), 22,559–22,574.

Wright, S. (2002), Well-sorted and graded sand is oscillatory sheet-flow, PhD thesis University of Aberdeen, Aberdeen, U. K.

Yu, X., T.-J. Hsu, and D. M. Hanes (2010), Sediment transport under wave groups: Relative importance between nonlinear waveshape and nonlinear boundary layer streaming, *J. Geophys. Res.*, *115*, C02013, doi:10.1029/2009JC005348.

Zyserman, J. A., and J. Fredsoe (1994), Data analysis of bed concentration of suspended sediment, *J. Hydraulic Eng.*, *120*(9), 1021–1042.